

# **Evidence in primates supporting the use of chemogenetics for the treatment of human refractory neuropsychiatric disorders**

Abbreviated title: Chemogenetic modulation of amygdala activity

PH Roseboom<sup>\*1</sup>, SAL Mueller<sup>\*1</sup>, JA Oler<sup>1</sup>, AS Fox<sup>2</sup>, MK Riedel<sup>1</sup>, VR Elam<sup>1</sup>, ME Olsen<sup>1</sup>, JL Gomez<sup>3</sup>, MA Boehm<sup>3</sup>, AH DiFilippo<sup>4</sup>, BT Christian<sup>4</sup>, M Michaelides<sup>3</sup>, and NH Kalin<sup>1</sup>

\* These authors contributed equally

Correspondence should be addressed to P.H.R. ([roseboom@wisc.edu](mailto:roseboom@wisc.edu))

<sup>1</sup> Department of Psychiatry and the HealthEmotions Research Institute, University of Wisconsin School of Medicine and Public Health, Madison, WI 53719

<sup>2</sup> Department of Psychology and the California National Primate Research Center, University of California-Davis, Davis, CA 95616

<sup>3</sup> Biobehavioral Imaging and Molecular Neuropsychopharmacology Unit, National Institute on Drug Abuse, Baltimore, MD 21224

<sup>4</sup> Department of Medical Physics, University of Wisconsin School of Medicine and Public Health, Madison, WI 53705

1    **Abstract**

2  
3    Non-human primate (NHP) models are essential for developing and translating new treatments  
4    that target neural circuit dysfunction underlying human psychopathology. As a proof-of-concept  
5    for treating neuropsychiatric disorders, we used a NHP model of pathological anxiety to  
6    investigate the feasibility of decreasing anxiety by chemogenetically (DREADDs) reducing  
7    amygdala neuronal activity. Intraoperative MRI surgery was used to infect dorsal amygdala  
8    neurons with AAV5-hSyn-HA-hM4Di in young rhesus monkeys. *In vivo* microPET studies with  
9    [<sup>11</sup>C]-deschloroclozapine and postmortem autoradiography with [<sup>3</sup>H]-clozapine demonstrated  
10   selective hM4Di binding in the amygdala, and neuronal expression of hM4Di was confirmed with  
11   immunohistochemistry. Additionally, because of its high affinity for DREADDs, and its approved  
12   use in humans, we developed an individualized, low dose clozapine administration strategy to  
13   induce DREADD-mediated amygdala inhibition. Compared to controls, clozapine selectively  
14   decreased anxiety-related freezing behavior in the human intruder paradigm in hM4Di-  
15   expressing monkeys, while coo vocalizations and locomotion were unaffected. These results  
16   are an important step in establishing chemogenetic strategies for patients with refractory  
17   neuropsychiatric disorders in which amygdala alterations are central to disease  
18   pathophysiology.

19 **Introduction**

20 Anxiety disorders are among the most prevalent psychiatric illnesses, and despite  
21 currently available treatments, remain a major public health concern.<sup>1, 2</sup> As such, there is a  
22 critical need to develop novel and improved treatment strategies. Anxiety disorders frequently  
23 begin in childhood, and by using our young rhesus monkey model of pathological anxiety we  
24 identified the neural circuit and molecular substrates relevant to understanding the childhood  
25 risk to develop anxiety disorders.<sup>3-12</sup> The evolutionary relatedness of NHPs to humans enables  
26 an opportunity to perform proof-of-concept studies in this highly translational model<sup>13-18</sup> that is  
27 directly relevant to human psychiatric illnesses. Our NHP work, modeling pathological anxiety or  
28 anxious temperament (AT), has demonstrated involvement of the dorsal amygdala, including  
29 regions such as the central nucleus (Ce) and dorsal aspects of the basolateral nuclei.<sup>3, 5, 7, 19</sup>  
30 Here, to further investigate mechanisms underlying primate anxiety, and as a model for potential  
31 human use, we use DREADDs (Designer Receptors Exclusively Activated by Designer Drugs)  
32 to reversibly manipulate neurons within the dorsal amygdala.<sup>20-22</sup> Demonstrating the ability to  
33 manipulate neural circuits using chemogenetic methods to reduce NHP anxiety is an important  
34 step towards developing novel treatments for refractory psychiatric illnesses, including severe  
35 human anxiety disorders.

36 DREADDs provide the ability to regulate the function of select brain circuits, which could  
37 lead to the development of specific neural circuit interventions, enabling personalized treatment  
38 strategies.<sup>22</sup> The most common DREADD method uses viral vector mediated gene delivery to  
39 induce cellular expression of mutated muscarinic receptors (hM3Dq – activating, hM4Di –  
40 inhibiting) that are not responsive to endogenous acetylcholine.<sup>20</sup> The ability to modulate  
41 DREADD-expressing cells requires the administration of a DREADD-activating selective ligand.  
42 DREADDs, and other chemogenetic methods, are particularly suitable for potential human  
43 interventions as the modulation of specific neural circuits can be accomplished via the oral or

44 parenteral administration of DREADD-activating drugs. Establishing reliable DREADD methods  
45 in NHPs has been challenging and the work presented here builds on encouraging recent  
46 progress.<sup>23-34</sup>

47 The use of DREADDs in humans will require methods for the precise delivery of viral  
48 vectors to targeted brain regions, sufficient expression of DREADDs in neuronal populations, as  
49 well as DREADD-activating drugs that are acceptable for human use. Additionally, use of this  
50 technology in humans will benefit from the ability to validate *in vivo*, the location and success of  
51 virally mediated DREADD expression, which could be accomplished with DREADD-specific  
52 positron emission tomography (PET) scanning. While clozapine-*N*-oxide (CNO) was initially  
53 proposed as an ideal DREADD-activating drug with high affinity and selectivity for DREADD  
54 receptors, and has been extensively used in rodent studies (for review see <sup>35</sup>), recent  
55 pharmacokinetic evidence suggests that CNO has poor brain penetrance.<sup>36, 37</sup> Additionally,  
56 studies in rodents, humans, and NHPs demonstrate that CNO can be back-metabolized into  
57 clozapine.<sup>36-41</sup> Because clozapine has high brain penetrance<sup>36, 42</sup> and can activate DREADDs at  
58 low doses,<sup>20, 36</sup> it has been suggested that the effects of CNO are mediated, at least in part, by  
59 clozapine.<sup>36, 37</sup>

60 Here, in an effort to develop new treatments for pathological anxiety, as well as to further  
61 develop the framework for using DREADDs in NHPs, we: 1) performed *ex vivo*  
62 immunohistochemical and autoradiographic studies to validate hM4Di expression and ligand  
63 binding to the receptor in the primate amygdala, 2) confirmed *in vivo*, with [<sup>11</sup>C]-  
64 deschloroclozapine (DCZ) microPET imaging, successful viral infection and transduction  
65 resulting in hM4Di amygdala expression, 3) established individualized dosing strategies for  
66 clozapine to limit off-target effects, and 4) implemented a within- and between-subjects  
67 experimental design to test whether DREADD-mediated inhibition of dorsal amygdala neurons  
68 would lead to a reversible decrease in anxiety-related behaviors. These studies provide  
69 important insights into the feasibility of using circuit-specific interventions to treat psychiatric

70 illnesses that are not amenable to current treatments.

71 **Results**

72 **Establishing Viral Vector-mediated Expression of hM4Di-HA in the Rhesus Amygdala**

73 To demonstrate efficacy of the viral vector method, we performed experiments in two  
74 pilot animals with injections of AAV5-hSyn-HA-hM4Di into the amygdala. One animal (subject  
75 P1; see Supplemental Table 1 for definition of subject identifiers) received bilateral 24 µL  
76 injections into the dorsal amygdala, and 36 days later the brain was perfused and collected for  
77 immunohistochemical analysis (chromogenic DAB staining and immunofluorescence). In one  
78 hemisphere, stereological methods (see Supplemental Table 2 for details) were used in  
79 immunofluorescently-labelled sections to estimate the total number of transduced neurons in the  
80 central nucleus (including both the lateral and medial divisions) as well as the basal nucleus  
81 (including the magnocellular and intermediate divisions; see Figure 1A). Approximately 27% of  
82 all neurons in the analyzed portions of the basal nucleus expressed hM4Di-HA, with dorsal  
83 regions showing relatively high density of HA and NeuN co-labelling (see Figure 1B). This is in  
84 contrast to the central nucleus, where less than 2% of neurons expressed DREADDs, and co-  
85 labelling of HA and NeuN was sparsely distributed (see Figure 1B). The other hemisphere of  
86 subject P1 was used for electron microscopy analyses, which as previously published  
87 demonstrated robust expression of hM4Di-HA on the cell membrane.<sup>23</sup>

88 To assess receptor binding, another animal (subject P2) received a unilateral 24 µL  
89 injection of AAV5-hSyn-HA-hM4Di into the dorsal region of the amygdala, and 35 days after  
90 surgery the brain was flash frozen and coronally sectioned for *in vitro* autoradiography. As can  
91 be seen in Figure 2A-B, specific binding of [<sup>3</sup>H]clozapine was 2.4-fold greater in the hM4Di  
92 expressing amygdala (right hemisphere) compared to the uninjected amygdala (left  
93 hemisphere).

95     **Determining Clozapine Dosing for DREADD Experiments in Rhesus Monkeys**

96           To establish a dose of clozapine that is without significant effects on anxiety-related  
97 behaviors such as freezing, we administered vehicle, 0.1 mg/kg and 0.5 mg/kg clozapine IM  
98 (N=5/group) prior to exposure to 30 minutes of the NEC condition. A one-way ANOVA revealed  
99 a significant effect of dose on freezing behavior ( $F_{2,12}=7.97$ ,  $p < 0.01$ ). The 0.5 mg/kg dose of  
100 clozapine significantly decreased the duration of freezing ( $p < 0.01$ ), which was not the case at  
101 the 0.1 mg/kg dose (Figure 3). Similarly, there was a significant effect of dose on experimenter  
102 orient ( $F_{2,12}=5.25$ ,  $p < 0.05$ ). The 0.5 mg/kg dose of clozapine significantly decreased the  
103 duration of time spent orienting towards the experimenter ( $p < 0.05$ ), whereas this was not the  
104 case at the 0.1 mg/kg dose. There was no significant effect on the duration of locomotion ( $F_{2,12}$   
105 = 0.13,  $p = 0.88$ ).

106

107     **Establishing Individualized Doses of Clozapine for the DREADD Behavioral Experiment**

108           While the previous clozapine dose ranging experiment established that the 0.1 mg/kg  
109 dose, on average, was without significant effects on freezing behavior, we observed individual  
110 variation in response to the 0.1 mg/kg dose. Therefore, to reduce the potential for intrinsic  
111 effects of clozapine on behavior, during subject selection we assessed the effects of 0.03 and  
112 0.1 mg/kg clozapine on each animal's behavior to develop an individualized dosing strategy. For  
113 each pair of animals (control and experimental) the highest dose of clozapine that was without  
114 behavioral effects was chosen. The 0.03 mg/kg dose was selected for three of the pairs and the  
115 0.1 mg/kg dose was selected for the remaining two pairs (of note, one pair of animals received  
116 only vehicle and 0.1 mg/kg clozapine during pre-testing).

117           In the four pairs of animals that received both doses of clozapine, plasma levels of  
118 clozapine and norclozapine demonstrated significant dose-dependent increases (clozapine,  $t_7 =$   
119 8.49,  $p < 0.0001$ ; norclozapine,  $t_7 = 6.11$ ,  $p < 0.001$ ). The plasma clozapine levels (mean ±

120 SEM) at the 0.03 mg/kg and 0.1 mg/kg doses were  $4.8 \pm 1.2$  ng/ml and  $16.6 \pm 1.9$  ng/ml,  
121 respectively. Similarly, plasma norclozapine levels were  $0.34 \pm 0.06$  ng/ml and  $0.89 \pm 0.10$   
122 ng/ml, respectively. Plasma levels of CNO were below the detection limit of the assay.  
123 Additionally, these doses of clozapine significantly decreased NEC-induced plasma ACTH ( $F_{2,14}$   
124 = 6.88;  $p < 0.05$ ; Figure 4) and cortisol concentrations ( $F_{2,14} = 4.60$ ;  $p = 0.05$ ; Figure 4). Because  
125 of these effects on plasma ACTH and cortisol, these hormonal measures were not analyzed in  
126 the DREADD experiment. Also, because NEC-induced cortisol is a component of the AT score,  
127 we did not use this composite score in assessing the effects of DREADD-mediated amygdala  
128 inhibition.

129

### 130 **Assessing hM4Di-HA Expression in the Experimental Animals**

131 The 5 monkeys that were selected as the experimental subjects received bilateral  
132 infusions of AAV5-hSyn-HA-hM4Di, with gadolinium as a contrast agent, targeted towards the  
133 dorsal amygdala region containing the Ce, as well as the dorsal aspects of the basal and  
134 accessory basal nuclei. After completion of each infusion, an MRI scan was acquired to  
135 visualize the infusate delivery region. Post-infusion scans were used to create a map indicating  
136 the infusion region that was overlapping and shared across the 5 subjects (Figure 5B). This  
137 revealed an overlap in gadolinium diffusion in the dorsal amygdala region, including the Ce and  
138 middle to dorsal aspects of the basal and accessory basal nuclei.

139 After behavioral testing, two experimental animals (subjects E2 and E3) and one  
140 unoperated animal (subject C1, which was not part of this study but had a similar prior  
141 experience with testing and clozapine dosing,) underwent [ $^{11}\text{C}$ ]-DCZ microPET scanning to  
142 assess *in vivo* hM4Di expression and localization. [ $^{11}\text{C}$ ]-DCZ, a derivative of clozapine, has  
143 recently been shown to be an effective PET radioligand for visualizing DREADDs due to its high  
144 selectivity and specificity for the hM4Di receptor.<sup>34</sup> To quantitatively assess specific [ $^{11}\text{C}$ ]DCZ  
145 binding, distribution volume ratio (DVR) parametric images were derived using the cerebellum

146 as a nonspecific-binding reference region (see Supplemental Figure 2).<sup>43, 44</sup> Because of  
147 individual variation in brain [<sup>11</sup>C]DCZ binding observed across the three animals, images were  
148 scaled such that the specific binding (i.e., DVR) in the prefrontal cortex was matched across the  
149 images. We then subtracted the aligned and scaled images of the control animal from each of  
150 the hM4Di-HA animals' images. Figure 6 depicts the average of these two difference images,  
151 overlaid on a template MRI, demonstrating a 40-50% [<sup>11</sup>C]DCZ signal increase in the amygdala  
152 region of the hM4Di-HA animals.

153 The brain from an additional experimental animal (subject E1) was used to quantify  
154 hM4Di-HA expression in the dorsal amygdala region of both the left and right hemispheres  
155 using stereological methods. This histological analysis focused on the regions of the amygdalae  
156 derived from the MRI images of gadolinium diffusion, that overlapped across the 5 experimental  
157 subjects. Consistent with the overall pattern of expression observed in the tissue from subject  
158 P1, co-expression levels of NeuN and hM4Di-HA as assessed with immunofluorescence were  
159 greatest within the dorsal portions of the basal and accessory basal nuclei compared to lower  
160 levels in the Ce (see Figure 7). Focusing on these nuclei, co-labelling of neurons was counted in  
161 subsampled regions encompassing 200 x 200 x 10 µm volumes. These analyses of portions of  
162 the right and left amygdala revealed transduction efficiencies in the subsampled regions that  
163 varied, ranging up to 67% (refer to Supplemental Figure 3 for further details). Additionally, some  
164 hM4Di-HA expression was observed in the dorsal region of the lateral nucleus, with much  
165 sparser expression in other amygdala nuclei. Outside of the amygdala, sparse cell-body  
166 labelling was also observed in the anterior hippocampus and ventral putamen. We also  
167 examined some projection sites of the amygdala to understand the extent to which DREADDs  
168 are anterogradely transported and expressed in the projections of infected cells. Consistent with  
169 this, chromogenic labelling of the HA-tag revealed discernible fibers in the bed nucleus of the  
170 stria terminalis, sublenticular extended amygdala, and lateral septum (Supplemental Figure 4).

171

172 **hM4Di-HA Activation Decreases Anxiety-related Freezing Behavior in the NEC Context**

173       Increased freezing is the prominent behavioral response occurring during the NEC  
174 condition. Using a 2 X 2 design, we examined clozapine-induced changes in freezing behavior  
175 (clozapine minus vehicle) across Group (Control vs hM4Di-HA) and Session (Pre vs.  
176 Postsurgical testing). Results demonstrated no significant main effect of Group and no  
177 significant main effect of Session. However, there was a significant Group X Session interaction  
178 ( $F_{1,8} = 14.89$ ,  $p = 0.0048$ ), such that in hM4Di-HA animals, clozapine treatment produced a  
179 significant change in freezing duration after, as compared to before, viral vector infusion ( $p =$   
180 0.007; Figure 8). This was not the case in the control animals. We note an outlying data point in  
181 the hM4Di-HA group during the Pre-testing period (diamond symbol; Figure 8) and when  
182 removing the Pre and Post data from this animal and its cage-mate control the results remain  
183 significant (Group X Session interaction;  $F_{1,6} = 12.09$ ,  $p = 0.013$ ). Because of the potential for  
184 individual differences in response to clozapine and because different doses of clozapine were  
185 used for different pairs of animals, we also performed an analysis residualizing the freezing  
186 durations with the plasma clozapine levels for all Pre and Post behavioral sessions. This  
187 analysis did not change the findings when the entire sample was included (Group X Session  $F_{1,8}$   
188 = 16.87,  $p = 0.0034$ ) or when the outlying pair of animals was removed from the analysis (Group  
189 X Session  $F_{1,6} = 9.18$ ,  $p = 0.023$ ). We also note that clozapine and norclozapine plasma levels  
190 did not significantly differ between the Control and hM4Di-HA groups either prior to or after  
191 surgery.

192       Because we detected significant effects of hM4Di-HA activation on freezing during the  
193 NEC condition, we also examined the extent to which hM4Di-HA activation affected freezing  
194 during the Alone and Stare conditions during which freezing is much less prominent. An  
195 analysis of the clozapine-induced changes in freezing behavior (clozapine minus vehicle) across  
196 the three HIP conditions (Alone, NEC, and Stare) was restricted to the postsurgical data  
197 because data from the Stare condition was only collected during the postsurgical period. The

198 results demonstrated a significant main effect of Group such that the DREADD animals had an  
199 overall greater reduction in freezing behavior than Controls across all conditions ( $F_{1,8} = 10.63$ ;  $p$   
200 = 0.012). Also, there was a lack of a significant HIP condition X Group interaction ( $F_{2,16} = 1.93$ ,  $p$   
201 = 0.18), suggesting that hM4Di-mediated amygdala inhibition reduced freezing behavior across  
202 conditions. When examining each condition separately, hM4Di activation was associated with  
203 reductions in freezing (Alone,  $p = 0.073$ ; NEC,  $p = 0.018$ ; Stare,  $p = 0.0081$ ). The results were  
204 unaffected when residualizing for plasma clozapine levels (Group –  $F_{1,8} = 19.61$ ;  $p = 0.0022$ ;  
205 HIP Condition x Group –  $F_{2,16} = 0.76$ ,  $p = 0.48$ ).

206 We next assessed the effects of hM4Di-mediated amygdala inhibition on the prominent  
207 behaviors that occur during the Alone and Stare conditions. The analysis for the Alone condition  
208 compared clozapine-induced changes (clozapine minus vehicle) before and after surgery.  
209 Increases in coo vocalizations and locomotion commonly occur during the Alone condition, and  
210 neither of these were significantly affected by clozapine-induced hM4Di activation. Bark  
211 vocalizations and experimenter-directed hostility are the prominent behaviors that are elicited by  
212 the Stare condition. Postsurgical data for the Stare condition (clozapine minus vehicle) revealed  
213 that these behaviors were unaffected by hM4Di-mediated amygdala inhibition.

214        **Discussion**

215            In the present study, we demonstrate that activation of the inhibitory hM4Di in the dorsal  
216            amygdala with low dose clozapine significantly decreases NHP anxiety-related behavior.  
217            Autoradiographic studies validated that clozapine binds to hM4Di-HA receptors expressed in the  
218            amygdala, and immunohistochemical methods determined that neurons expressing these  
219            receptors were most prominently located in the dorsal regions of the basal and accessory basal  
220            nuclei. Advancing the translational utility of chemogenetics, we replicate the finding that [<sup>11</sup>C]-  
221            DCZ microPET scanning can be used to visualize DREADD expression *in vivo*<sup>34</sup>, revealing  
222            selective binding in the viral vector targeted regions of the amygdala.

223            Because clozapine has affinity for many endogenous receptors and is well known to  
224            have behavioral effects,<sup>45, 46</sup> and because we observed individual differences in responses at  
225            low doses, we used an individually determined dosing approach in the DREADD experiment.  
226            The goal of the individualized approach was to identify the highest dose of clozapine that was  
227            without off-target behavioral effects. Animals were tested in pairs (experimental and control) and  
228            the same dose was selected for further experimentation in each pair. Thus, optimal and identical  
229            dosing was used for each member of each pair of animals. There was no significant difference  
230            in plasma levels between control and experimental subjects because the experimental animal  
231            and its paired control received the same dose of clozapine. Additionally, we used plasma levels  
232            in the behavioral analyses to control for any potential pharmacokinetic differences between  
233            animals.

234            The findings demonstrated a significant clozapine-induced decrease in freezing behavior  
235            in the hM4Di-HA subjects during NEC, a threat-related context in which the predominant  
236            response is to freeze. In addition to the effects observed during NEC, hM4Di activation also  
237            reduced freezing during the Alone and Stare conditions. No significant effects of DREADD  
238            activation were observed for other behaviors including coo or bark vocalizations, locomotion, or  
239            experimenter-directed hostility. The effects of hM4Di-induced amygdala inhibition on freezing

240 are consistent with previous publications examining the effects of amygdala lesions on threat-  
241 related responses in NHPs and rodents.<sup>19, 47, 48</sup>

242 A previous study used clozapine and CNO to examine the impact of hM4Di-HA  
243 DREADD-mediated amygdala inhibition on anxiety-related behavior during the HIP in two young  
244 rhesus monkeys.<sup>31</sup> While no control group was included in the DREADD behavioral analyses,  
245 this study reported decreased drug-induced (CNO and clozapine) freezing during the HIP with  
246 no changes in vocalizations, which is consistent with our findings. In another study using CNO,  
247 DREADD-induced amygdala inhibition in adult rhesus monkeys resulted in reductions in  
248 amygdala-frontal cortex resting-state functional connectivity.<sup>27</sup> This finding is interesting in  
249 relation to our demonstration of a DREADD-induced reduction in threat-related freezing  
250 behavior as the circuit disruptions reported by Grayson et al, overlap with regions implicated in  
251 mediating primate threat-related anxiety.<sup>7, 49</sup> This study also did not use a non-DREADD control  
252 group as a comparator, leaving open the possibility that the observed effects could be due to  
253 the intrinsic actions of CNO and/or its back metabolism to clozapine, and not to DREADD  
254 activation *per se*.

255 In the present study we used gadolinium as an MRI contrast agent during the viral vector  
256 infusion to intraoperatively observe the extent of the infusion. Previous studies utilizing  
257 gadolinium to monitor viral infusions have shown that *in vivo* assessment of gadolinium  
258 distribution can predict the distribution of protein expression resulting from AAV-mediated  
259 infection.<sup>50, 51</sup> Consistent with this, our histochemical characterization of a DREADD behavioral  
260 study subject demonstrated considerable expression in the dorsal portions of the basal and  
261 accessory basal nuclei. A similar expression pattern was observed in the pilot subject. While we  
262 assume that the expression is similar in the four additional experimental animals, this remains to  
263 be confirmed.

264 Based on the predominance of DREADD expression in the dorsal regions of the basal  
265 and accessory basal nuclei and the known functions of these nuclei, it is plausible that the

266 infected neurons in these regions mediated the reductions in threat-related freezing behavior.  
267 The basal and accessory basal nuclei are primarily composed of glutamatergic projection  
268 neurons, along with a smaller population of GABAergic interneurons.<sup>52-54</sup> Because our DREADD  
269 construct utilized the synapsin promoter, both of these cell types were likely infected. The basal  
270 and accessory basal nuclei receive sensory input from the thalamus and the cortex as well as  
271 higher order information from the hippocampus and PFC<sup>55, 56</sup>, and send outputs to the Ce, BST,  
272 striatum, hypothalamus, hippocampus, and PFC.<sup>57-60</sup> Many rodent studies have demonstrated  
273 that these amygdala subregions are involved in modulating anxiety-related behavior.<sup>60-67</sup> For  
274 example, inhibition of basolateral projections to ventral hippocampus have been shown to  
275 decrease anxiety-related behaviors,<sup>66</sup> whereas inhibition of basolateral projections to the lateral  
276 division of the Ce have been shown to increase anxiety-related behaviors.<sup>67</sup> Furthermore,  
277 human imaging studies further implicate a role for basal, accessory basal and lateral nuclei  
278 (considered together as the basolateral amygdala (BLA)) dysfunction in psychiatric disorders, as  
279 disruptions in BLA functional connectivity are observed in patients with generalized anxiety  
280 disorder.<sup>68</sup>

281 In addition to the considerable expression in the dorsal basal and accessory basal  
282 nuclei, a low level of DREADD expression was observed in the Ce. The Ce consists primarily of  
283 GABAergic neurons and is considered the major output nucleus of the amygdala.<sup>69</sup> In addition,  
284 our previous mechanistic and neuroimaging work has implicated the Ce as a key node in the  
285 neural network underlying the expression of AT.<sup>70</sup> It is conceivable that the modulation of a  
286 small number of neurons in the Ce is sufficient to induce alterations in behavior. Other work in  
287 NHPs has demonstrated that DREADD transduction levels as low as 3% of neurons in the  
288 dorsolateral PFC appears to be effective at influencing spatial working memory.<sup>29</sup> Thus, in  
289 addition to the probable contribution of the dorsal basal and accessory basal nuclei, it is  
290 possible that the small number of Ce neurons expressing hM4Di could be contributing to the  
291 behavioral effects observed here. Of further consideration, some hM4Di expression was

292 observed in neurons located between the basal and accessory basal nuclei and the Ce. This is  
293 potentially important because the GABAergic neurons found in this region, which constitute the  
294 intercalated cell masses, act as an inhibitory gate for information flowing from the BLA to the  
295 Ce.<sup>71, 72</sup>

296 The sparsity of Ce hM4Di expression found in the present study is consistent with data  
297 from other reports in primates using AAV2 or AAV5 infused into the amygdala.<sup>27, 51, 73</sup>  
298 Interestingly, in rodent studies AAV5 has been successfully utilized to infect the Ce.<sup>74-76</sup> Other  
299 data from our laboratory (S.A.L.M. and N.H.K., unpublished data) suggests that various AAV  
300 vectors, specifically AAV8, and AAV9, also show scarce Ce infectivity in primates. Studies  
301 aimed at characterizing the role of the NHP Ce will require the identification of methods that  
302 more robustly infect NHP Ce neurons.

303 Overall, our findings demonstrate the utility of using DREADD technology in NHPs to  
304 investigate the neural circuitry underlying the expression of anxious behavior and further  
305 highlight the importance of the amygdala in threat-related responding. In future studies,  
306 chemogenetic technology could be similarly applied to functionally define the role of other  
307 cortical and subcortical components of the neural circuitry underlying primate anxiety. The  
308 implementation of chemogenetic technology in this NHP model sets the stage for the possibility  
309 of using DREADDs to identify and develop novel clinical interventions targeting specific cell  
310 types within specific regions of the neural circuits that underlie human pathological anxiety.

311 **Materials and Methods**

312 **Experimental Model and Subject Details**

313 Studies were performed using male and female rhesus monkeys (*Macaca mulatta*), with the  
314 gender composition and age ranges as described for each study in the methodological details  
315 below. Monkeys were housed and cared for at the Wisconsin National Primate Research Center  
316 and the Harlow Center for Biological Psychology on a 12-hour light/dark cycle, in a temperature-  
317 and humidity-controlled vivarium. Procedures were performed using protocols that were  
318 approved by the University of Wisconsin Institutional Animal Care and Use Committee in  
319 compliance with the Guide for the Care and Use of Laboratory Animals published by the US  
320 National Institutes of Health.

321

322 **Assessing behavioral effects of clozapine**

323 Prior to beginning studies using the DREADD virus, we assessed whether low doses of  
324 clozapine administered to control subjects would impact the level of anxiety-like responding  
325 during the No-Eye-Contact (NEC) condition of the Human Intruder Paradigm (HIP)<sup>3, 12, 77</sup>. Using  
326 a between-subjects design (N = 5/grp; males, mean age at time of behavioral testing = 2.03 ±  
327 0.07 years), monkeys were treated with either vehicle, 0.1 mg/kg clozapine or 0.5 mg/kg  
328 clozapine. The solutions used for the 0.1 mg/kg and 0.5 mg/kg doses were prepared at a  
329 concentration of 0.2 mg/ml and 1 mg/ml, respectively, by dissolving the clozapine in DMSO and  
330 then diluting in 0.9% saline to a final DMSO concentration of 25%. The drug was administered  
331 as bilateral intramuscular injections at a volume of 0.5 ml/kg. Vehicle injected animals received  
332 0.5 ml/kg of 25% DMSO in 0.9% saline. Drug or vehicle was administered 40 min prior to  
333 exposure to 30 min of NEC. The duration of freezing behavior, which was defined as a lack of  
334 movement for greater than 3-seconds, the duration of locomotion, which was defined as  
335 ambulation of one or more steps at any speed, and the duration of experimenter orient, which

336 was defined as any non-hostile orienting behavior toward the experimenter, were recorded in  
337 seconds.

338

339 **AAV5-hSyn-HA-hM4Di DREADDs subjects**

340 The timeline for behavioral testing of subjects is shown in Figure 5A. To maximize the potential  
341 for observing the hypothesized decrease in freezing resulting from the DREADDs receptor  
342 activation, monkeys were initially screened with 10 min of NEC to identify and select mid- to  
343 high-level freezers. Of the ninety-four animals that were screened (47 males/47 females, mean  
344 age at time of screening  $1.83 \pm 0.08$  years), sixteen were then chosen to be tested for  
345 responsiveness to clozapine. Animals were tested using 10 min of Alone followed by 10 min of  
346 NEC following administration of vehicle, 0.03 mg/kg clozapine and 0.1 mg/kg clozapine. One  
347 pair of animals received only the 0.1 mg/kg dose of clozapine during the clozapine  
348 responsiveness testing. The solutions used for the 0.03 mg/kg and 0.1 mg/kg clozapine doses  
349 had concentrations of 0.06 mg/ml or 0.2 mg/ml, respectively, and were prepared and  
350 administered as described in the preceding section (Assessing behavioral effects of clozapine).  
351 Drug or vehicle was administered 30 min prior to behavioral testing. At the conclusion of the  
352 test, blood was collected to assess the impact of clozapine on plasma ACTH and cortisol levels  
353 and measurement of plasma clozapine and norclozapine levels. All blood collections were done  
354 at the same time of day (range 8:43 AM – 11:05 AM). To obtain plasma, blood was collected in  
355 EDTA tubes and immediately centrifuged at 1,900 x g for 10 min at 4°C and the supernatant  
356 collected. Tests were separated by one week and the order was randomized. Animals that  
357 showed a pronounced clozapine-induced decrease in freezing during the NEC even at the low  
358 dose were not used further in the study. Ultimately, 10 animals were chosen for surgery or to  
359 serve as matched unoperated control subjects (6 males and 4 females, mean age at time of  
360 surgery =  $2.19 \pm 0.23$  years). The clozapine testing procedure also determined the dose of  
361 clozapine used in the post-surgery testing. We chose the highest dose of clozapine that did not

362 substantially affect freezing behavior in the NEC, which for two pairs of animals was 0.1 mg/kg  
363 and for the other three pairs was 0.03 mg/kg.

364 Post-surgical testing began approximately 32 days after surgery (see Figure 5A). The  
365 clozapine preparation and injection methods were the same as for the screening procedure.  
366 Drug or vehicle was administered 30 min prior to behavioral testing. Behavioral testing was  
367 performed using the human intruder paradigm (HIP), which consisted of 10 min of Alone, 10 min  
368 of NEC, 5 min of Alone, 10 min of Stare and ending with 15 min of Alone followed by blood  
369 collection for measurement of plasma clozapine and norclozapine levels. All blood collections  
370 were done at the same time of day (range 9:10 AM – 11:07 AM). Subjects were tested with  
371 vehicle and either 0.03 mg/kg or 0.1 mg/kg clozapine based on the results from the screening  
372 tests. Postsurgical behavioral testing was performed with randomized drug and vehicle  
373 administration separated by at least 2 weeks. Subjects received a second round of testing  
374 approximately 32 days later with counterbalanced drug and vehicle administration, again  
375 separated by at least 2 weeks. Prior to statistical analysis, the results were averaged across the  
376 two rounds of testing.

377 The HIP assesses monkeys in three different contexts eliciting different defensive  
378 responses. The HIP begins with the Alone condition, during which a monkey is separated from  
379 its cage-mate and is placed into a test cage by itself. This context typically elicits separation  
380 behaviors such as coo-vocalizations and increases in locomotion. The Alone condition is  
381 followed by the NEC condition wherein a human intruder enters the room and presents her/his  
382 profile to the monkey, while avoiding direct eye contact. Responses to this potentially  
383 threatening situation include increases in freezing, decreases in locomotion and decreases in  
384 coo vocalizations. The final context is the Stare condition, during which the intruder reenters the  
385 room and stares directly at the monkey, eliciting hostile behaviors directed towards the intruder  
386 (i.e., bark vocalizations and experimenter-directed hostility).

387

388 **Assessing neuroendocrine effects of clozapine**

389 To examine the effects of clozapine dose on HPA axis function following 10 min of Alone and 10  
390 min of NEC exposure, plasma levels of cortisol and ACTH were assessed. **ACTH assay:**  
391 Plasma samples were assayed for ACTH using the MD Biosciences (Oakdale, MN) enzyme-  
392 linked immunosorbent assay (ELISA) following the manufacturer's instructions. Samples were  
393 assayed in duplicate. The inter-assay CV%<sup>s</sup> were calculated for a low and a high control  
394 sample. The low control had an average value of  $41.7 \pm 0.8$  pg/ml and a CV% of 9.0 and the  
395 high control had an average value of  $249.4 \pm 4.2$  pg/ml and a CV% of 7.8. The limit of detection  
396 defined by the lowest standard was 5 pg/ml. **Cortisol assay:** Plasma samples were assayed for  
397 cortisol in duplicate using the MP Biomedicals (Solon, OH) Immuchem coated tube  
398 radioimmunoassay. The intra-assay CV% was 4.9 and the inter-assay CV% was 9.8. The  
399 detection limit defined by the lowest standard was 1  $\mu$ g/dL.

400

401 **Assessing plasma levels of clozapine and its metabolites**

402 Plasma levels of clozapine and its metabolites norclozapine and clozapine-N-oxide were  
403 measured using HPLC coupled with mass spectroscopy as previously described.<sup>30</sup> The plasma  
404 aliquots used were collected at the conclusion of the behavioral tests. A Nexera XR HPLC  
405 (Shimadzu, Kyoto, Japan) coupled with a QTRAP 6500 (SCIEX, Redwood City, CA) was used  
406 to acquire data that was analyzed with Analyst 1.6 (SCIEX).

407

408 **Surgical procedures**

409 **Trajectory guide base placement and intraoperative MRI**

410 The placement of the trajectory guide bases followed published methods<sup>78, 79</sup> that were modified  
411 to target the dorsal amygdala following procedures described in supplemental methods section  
412 of two previous publications<sup>51, 73</sup> with slight modifications. To cover as much of the dorsal  
413 amygdala (central nucleus (Ce) and dorsal aspects of the basal and accessory basal nuclei) as

414 possible while minimizing infection of the surrounding tissue, one 24  $\mu$ l infusion was performed  
415 per hemisphere. In an effort to maximize coverage of the dorsal amygdala, the 24  $\mu$ l was  
416 injected over multiple infusions with adjustments made to injector depth based on information  
417 obtained from the intraoperative MRI scans collected between infusions. As can be seen in  
418 Figure 5B, this ensured that the animals all received the DREADDs virus in an overlapping  
419 region of the dorsal amygdala.

420

421 Before the procedure, the animals were anesthetized with ketamine (up to 20 mg/kg,  
422 intramuscular (IM)), prepared for surgery, and then placed in an MRI compatible-stereotaxic  
423 frame. The animals were intubated and received isoflurane anesthesia (1 – 3%, intratracheal)  
424 with 1-1.5% O<sub>2</sub> administered during induction. Atropine sulfate (0.01 – 0.4 mg/kg, IM) was  
425 administered to depress salivary secretion, and buprenorphine (0.01 – 0.03 mg/kg, IM, repeated  
426 every 6 – 12 hours) was given for analgesia. To maintain fluids and electrolytes, Plasmalyte (up  
427 to 10 mg/kg/hr, intravenous (IV)) was administered. Cefazolin (20 – 25 mg/kg, IM or IV) was  
428 administered as a prophylactic antibiotic one day prior to the surgery. Cefazolin was also  
429 administered immediately prior to surgery, and then every 6 hours while under anesthesia. All  
430 drugs and treatments were given in consultation with veterinary staff. Vital signs (heart rate,  
431 respiration, oxygen saturation, and end tidal CO<sub>2</sub>) were continuously monitored. Body  
432 temperature was monitored during the surgical and MRI procedure and maintained in the MRI  
433 by wrapping the animals for warmth while incorporating a hot water heating device within the  
434 wrap.

435

#### 436 **Cannula trajectory planning and insertion**

437 Cannula trajectory planning was carried out in the MRI suite under anesthesia as previously  
438 described.<sup>73</sup> The infusion line was primed with a loading line solution that was identical to the  
439 virus suspension solution [Dulbecco's phosphate-buffered saline (D-PBS) without Ca<sup>2+</sup> or Mg<sup>2+</sup>

440 (Gibco, ThermoFisher Scientific, Waltham, MA) containing 0.001% F68 surfactant (Gibco,  
441 ThermoFisher Scientific)], and the cannula was loaded with the DREADDs viral vector and the  
442 MR visible marker Gadobenate dimeglumine (Gd, MultiHance; Bracco Diagnostics, Monroe  
443 Township, NJ). The pilot subject and four out of the five experimental subjects had a 100 mm  
444 length valve tip cannula (Engineering Resources Group, Pembroke Pines, FL) with a fused  
445 silica cannula having a polyimide tubing tip that was sealed with a retractable glass fiber stylet.  
446 Its dimensions were: tip—outer diameter (OD) = 0.40 mm, inner diameter (ID) = 0.345 mm,  
447 length = 3.0 mm; shaft—OD = 0.67 mm, ID = 0.45 mm, length = 97.0 mm from ferrule; stylet—  
448 OD = 0.275 mm. One subject had a 100 mm length cannula (Engineering Resources Group)  
449 with a fused silica single-end port cannula with OD = 0.67 mm and ID = 0.45 mm.

450 After the pressure in the infusion line was stabilized, the cannula was introduced into the  
451 brain, advancing the remote introducer at approximately 10 – 15 mm/minute. The cannula was  
452 advanced two-thirds of the measured depth towards the target for partial insertion, and another  
453 targeting 3D T1W MRI was performed to confirm the correct trajectory and calculate the  
454 remaining distance from cannula tip to target. Once confirmed, the cannula was advanced to its  
455 final position and the stylet was retracted. When the pressure reading on the infusion pump  
456 controller system stabilized, the infusion began.

457 The infusate consisted of AAV5-hSyn-HA-hM4Di suspended in a solution identical to the  
458 loading line solution described above. To facilitate *in vivo* MRI visualization of the infusion, Gd  
459 was mixed with the viral vector at a final concentration 0.66 mM. In the pilot subject used for  
460 autoradiographic experiments, a total volume of 24  $\mu$ l was infused unilaterally into the right  
461 dorsal amygdala region at a steady rate of 1  $\mu$ l/min. In each of the five DREADDs behavioral  
462 experiment subjects a total volume of 24  $\mu$ l per hemisphere was bilaterally infused into the  
463 dorsal amygdala region at a steady state rate of 1  $\mu$ l/min, except for one experimental monkey  
464 where the infusion into the right hemisphere was 3  $\mu$ l/min to improve cannula flow possibly due  
465 to a clogged injector. After each infusion, another 3D MRI scan was reacquired for a qualitative

466 visualization of the volumetric infusate delivery region. This sequence provides sensitivity to the  
467 contrast-enhanced infusate and sufficient gray/white contrast for easy identification of the  
468 infusion's anatomical location. These post infusion scans were used to create the infusion  
469 overlap image in Figure 5B. After the infusions were complete the animal was transported back  
470 to the surgical suite. To reduce intracranial pressure and prevent brain swelling, Mannitol (up to  
471 2.0 g/kg, IV) was given as needed. The trajectory guides were removed, and the incision was  
472 closed in layers before the animal was allowed to recover from anesthesia. Animals were given  
473 buprenorphine twice on the day following the surgery (0.01-0.03 mg/kg, IM). Cefazolin (20-25  
474 mg/kg, IM or IV) or Cephalexin (20-25 mg/kg, oral (PO)) was given twice daily for five days after  
475 surgery to prevent infection. The animals were allowed to recover, and testing did not  
476 commence until 28 to 35 days (average 32 days) after surgery.

477

#### 478 **Viral vectors**

479 Monkeys received infusions of the DREADD viral vector AAV5-hSyn-HA-hM4Di obtained from  
480 the Boston Children's Hospital Viral Core Facility (Boston, MA). The lot of virus used for the pilot  
481 subject had a titer of  $6.95 \times 10^{13}$  genome copies /ml, and the lot of virus used for the five  
482 experimental subjects had a titer of  $6.28 \times 10^{13}$  genome copies/ml. The construct plasmid map  
483 (pOTTC1484, Addgene, Watertown, MA) is shown in Supplemental Figure 1.

484

#### 485 **Validation of hM4Di-HA expression *ex vivo***

##### 486 ***[<sup>3</sup>H]Clozapine autoradiography***

487 Autoradiography with [<sup>3</sup>H]Clozapine was used to demonstrate DREADD ligand binding in tissue  
488 sections obtained from the amygdala. Thirty-five days following surgery subject P2 was  
489 euthanized, the brain was removed and the region containing the amygdala was cut coronally  
490 into a 21 mm thick slab that was then flash frozen in chilled isopentane (ThermoFisher  
491 Scientific) maintained on dry ice. The tissue was then sectioned at 20  $\mu$  thickness and mounted

492 onto Superfrost Plus microscope slides (ThermoFisher Scientific) and stored at -80°C until use.  
493 For the assay, sections from the left and right hemisphere were matched in the coronal plane  
494 using acetylcholinesterase (AChE), a cholinergic marker that can identify nuclei within the  
495 amygdala<sup>80, 81</sup>. Autoradiography using [<sup>3</sup>H]clozapine was then performed following a published  
496 protocol described in detail in the supplemental methods section accompanying a previous  
497 publication starting with the preincubation step.<sup>36</sup> The image generated by the phosphorimager  
498 (Typhoon, FLA 7000, GE Healthcare, Piscataway, NJ) was quantified using Multi Gauge v.3  
499 software (Fuji Photo Film, Tokyo, Japan) by drawing a region of interest around the amygdala  
500 on the uninjected left hemisphere and the injected right hemisphere. Values were averaged and  
501 expressed as nCi/g with the use of Carbon-14 standards (American Radiolabeled Chemicals  
502 Saint Louis, MO) exposed and imaged on the same phosphor screen as the experimental  
503 slides. For each hemisphere, the specific [<sup>3</sup>H]clozapine binding in the amygdala was obtained  
504 by subtracting the non-specific signal obtained in the presence of excess cold clozapine (100  
505 μM) from the total [<sup>3</sup>H] clozapine signal. Three tissue sections per hemisphere were used for the  
506 total [<sup>3</sup>H] clozapine binding condition, while one tissue section per hemisphere was used for the  
507 non-specific binding condition.

508

#### 509 **Immunohistochemical procedures**

#### 510 **HA-Tag Expression**

511 Time between surgery and necropsy was 36 days for subject P1 and 434 days for subject E1.  
512 Animals were euthanized by transcardial perfusion with heparinized PBS at room temperature  
513 followed by fixation with 4% paraformaldehyde (PFA) in PBS at 4 °C. In the case of subject P1,  
514 which was also used for electron microscopy studies, perfusion was performed using ice-cold,  
515 oxygenated Ringer's buffer followed by 4% PFA containing 0.1% glutaraldehyde in 0.2 M  
516 phosphate buffer, pH 7.4. Brains were removed and fixation was continued in the perfusion  
517 solution overnight at 4 °C. The brains were placed in a brain block and cut into slabs that were

518 subsequently processed through increasing concentrations of sucrose –10%, 20% and 30%.  
519 The approximately 14 mm thick tissue slab containing the amygdala was frozen and cut at 40  
520 microns on a cryostat (CryoStar NX50, ThermoFisher Scientific). Tissue sections were stored in  
521 cryoprotectant (40 mM potassium phosphate/11mM sodium phosphate buffer, pH 7.2,  
522 containing 30% ethylene glycol and 30% sucrose) at -20 °C until use.

523 To observe hM4Di-HA expression within the amygdala as well as its putative projection  
524 sites, chromogenic labeling of HA-tag was performed. Tissue sections were washed overnight  
525 with PBS to remove cryoprotectant, and all subsequent incubations were carried out at room  
526 temperature in PBS containing 0.3% Triton X-100. Three 5-minute washes with PBS were  
527 performed in between each incubation step. To block endogenous peroxidase activity, tissue  
528 sections were first incubated in PBS containing 6% hydrogen peroxide for 30 minutes. Sections  
529 were then blocked in 5% normal goat serum (Cat # S-1000; Vector Laboratories, Burlingame,  
530 CA) for one hour. This was followed by an overnight incubation with a 1:400 dilution of rabbit  
531 monoclonal HA-tag antibody (C29F4, Cat # 3724; Cell Signaling Technology, Danvers, MA),  
532 and a one-hour incubation with a 1:250 dilution of Peroxidase-conjugated goat anti-rabbit IgG  
533 secondary antibody (Cat #PI-1000; Vector Laboratories). A 2-minute incubation with ImmPACT  
534 DAB (3,3'-Diaminobenzidine) peroxidase substrate (Cat # SK-4105; Vector Laboratories) was  
535 then used for visualization. Sections were mounted on Superfrost Plus microscope slides, which  
536 were air-dried, dehydrated in 95% and then 100% ethanol, and placed in xylene for 5 minutes  
537 before coverslipping with DPX mounting medium. Images were captured using a DM6000B light  
538 microscope (Leica Microsystems, Buffalo Grove, IL).

539 To identify neurons that were expressing hM4Di-HA, immunofluorescent co-labelling of  
540 HA-tag and neuronal nuclei (NeuN) was performed (Figure 5C). Tissue sections were washed  
541 overnight with PBS to remove cryoprotectant, and all subsequent incubations were carried out  
542 at room temperature in PBS containing 0.3% Triton X-100. Three 5-minute washes with PBS  
543 were performed in between each incubation step. Tissue sections were first blocked in 5%

544 normal goat serum (Cat # S-1000; Vector Laboratories, Burlingame, CA) for one hour. This was  
545 followed by an overnight incubation with a 1:400 dilution of rabbit monoclonal HA-tag antibody  
546 (C29F4, Cat # 3724; Cell Signaling Technology, Danvers, MA), and a one-hour incubation with  
547 a 1:250 dilution of Alexa Fluor 488 conjugated goat anti-rabbit secondary antibody (Cat #  
548 A11008; ThermoFisher Scientific). Tissue sections were then blocked in 5% normal donkey  
549 serum (Cat # 017-000-121; Jackson ImmunoResearch, Laboratories, Inc., West Grove, PA).  
550 This was followed by an overnight incubation with a 1:2000 dilution of mouse monoclonal NeuN  
551 antibody (clone A60, Cat # MAB377; MilliporeSigma, Darmstadt, Germany), and a one-hour  
552 incubation with a 1:250 dilution of Alexa Fluor 647 conjugated donkey anti-mouse secondary  
553 antibody (Cat # A31571; ThermoFisher Scientific) Cellular nuclei were stained using a 1:10000  
554 dilution of 4',6-diamidino-2-phenylindole (DAPI) for 5 minutes. Sections were mounted on  
555 Superfrost Plus microscope slides using ProLong Gold Antifade Mountant (Cat # P36930;  
556 ThermoFisher Scientific).

557

#### 558 **Imaging and Stereological Quantification of Expression**

559 For subject P1, 1:15 coronal sections through the central nucleus, or 1:30 coronal sections  
560 through the basal nucleus, were sampled for analysis of HA-tag and NeuN co-expression. For  
561 subject E1, 1:10 coronal sections through the amygdala were sampled for analysis of HA-tag  
562 and NeuN co-expression. Sections immediately adjacent to these were processed for  
563 acetylcholinesterase (AChE), a cholinergic marker that was used to identify nuclei within the  
564 amygdala.<sup>80, 81</sup> Fluorescent image stacks were acquired using a A1R-Si+ confocal microscope  
565 (Nikon Instruments, Melville, NY) with a pan fluor 40x oil objective (1.30 N.A.) and Nikon NIS-  
566 Elements software. Section thickness was measured by focusing on the top of each tissue  
567 section, refocusing to the bottom of the tissue section, and then measuring the difference in Z-  
568 axis. All sections were imaged using the same acquisition settings, including magnification,  
569 laser power, camera gain, offset, pinhole size, and scan speed.

570 To evaluate neuronal expression of HA-DREADDs, standard unbiased stereological  
571 counting of HA and NeuN immunopositive cells was accomplished with the optical fractionator  
572 workflow in Stereo Investigator software (MBF Bioscience). For further details concerning the  
573 stereological parameters used, see Supplemental Table 2. Counting was performed by a single  
574 trained investigator.

575 Pilot studies were used to determine the appropriate counting parameters, such that  
576 there would be a sufficient number of neurons in each counting frame to allow for meaningful  
577 interpretation of percentage of neurons expressing hM4Di-HA in a given subsampled region.  
578 Cells that were immunoreactive for NeuN and HA-tag were identified using the soma as the  
579 counting target. Cells with a well-defined soma and nucleus were counted if they were within or  
580 intersecting with the disector frame and not intersecting with lines of exclusion.

581

### 582 **[<sup>11</sup>C]DCZ Radiosynthesis**

583 The [<sup>11</sup>C]deschloroclozapine was synthesized similar to published methods <sup>34</sup> with  
584 modifications. The radiolabeling synthon, [<sup>11</sup>C]methyl triflate was produced using the gas phase  
585 method, starting with the production of [<sup>11</sup>C]methane via the <sup>14</sup>N(*p*,*a*)<sup>11</sup>C nuclear reaction using a  
586 90/10 H<sub>2</sub>/N<sub>2</sub> target.<sup>82</sup> The [<sup>11</sup>C]methane was converted to [<sup>11</sup>C]methyl iodide through gas phase  
587 iodination with iodine vapor in a heated quartz tube using a recirculation process.<sup>83</sup> [<sup>11</sup>C]MeI was  
588 then passed through a heated glass tube containing silver triflate for the production of  
589 [<sup>11</sup>C]methyl triflate.<sup>82</sup> The [<sup>11</sup>C]MeOTf was slowly bubbled into a reaction vial containing 0.2mg  
590 11-(1-Piperazinyl)-5H-dibenzo[b,e][1,4]diazepine precursor (Tocris, Bio-Techne Corp.,  
591 Minneapolis, MN) and 0.3mL anhydrous MeCN. The radiolabeling reaction occurred at room  
592 temperature for 5 minutes, after which 0.5 mL mobile phase was added to the vial and the entire  
593 solution injected onto the semi-preparative HPLC system. The semi-preparative HPLC system  
594 consists of a Waters 515 HPLC pump (5 mL/min), Waters 2489 UV Detector (254 nm),  
595 Phenomenex Gemini NX C-18 column (250 mm x 10 mm), and a mobile phase composed of

596 MeCN/H<sub>2</sub>O/Et<sub>3</sub>N (40/60/0.1%). The peak corresponding to [<sup>11</sup>C]DCZ was collected and diluted  
597 in 60 mL water and trapped on a tC18 light cartridge (Waters, Milford, MA) which was then  
598 rinsed with 10 mL 0.002N HCl. The [<sup>11</sup>C]DCZ compound was then eluted from the cartridge  
599 using 0.5 mL EtOH and 10 mL 0.9% sodium chloride, USP through a Millex-FG membrane filter  
600 (MilliporeSigma, Darmstadt, Germany). The purity of the tracer was verified using a  
601 Phenomenex Luna C18 column (200 mm x 4.6 mm) and mobile phase of MeCN/H<sub>2</sub>O/Et<sub>3</sub>N  
602 (40/60/0.1%) with a flow rate of 2 mL/min. No radiochemical or chemical impurities were  
603 observed. The specific activity was 29.3±15.3 mCi/nmol at end of synthesis (N = 4).

604

#### 605 **PET Scanning**

606 The subjects were anesthetized with ketamine (15 mg/kg, IM), given atropine sulfate (0.04  
607 mg/kg, IM) to depress salivary secretion, intubated and received isoflurane anesthesia (1–1.5%,  
608 IT), and placed in the Focus 220 microPET scanner in the prone position with the head facing  
609 downward and secured in a custom-made head holder. Throughout the experimental procedure  
610 vital signs (heart rate, respiration, oxygen saturation, end tidal CO<sub>2</sub>, and body temperature) were  
611 continuously monitored. To maintain fluids and electrolytes, Plasmalyte (up to 10 mg/kg/hr, IV)  
612 was administered. A transmission scan was acquired for 518 seconds using a <sup>57</sup>Co rotating rod  
613 source to correct for the scatter and attenuation of radiation in the tissue. The PET scan was  
614 initiated with the injection of the [<sup>11</sup>C]DCZ (N=4.85mCi ± 0.23 mCi; 0.12 ± 0.06 micrograms  
615 DCZ). The list mode emission data was acquired for a total of 90 minutes and binned into a time  
616 series of 22 frames: 2 x 1 min, 4 x 2 min, 16 x 5 min. The PET data were reconstructed using  
617 filtered back-projection and a ramp filter into a matrix size of 128 x 128 x 95 with voxel  
618 dimensions of 0.959mm x 0.959mm x 0.796mm. We note that four animals were scanned, two  
619 with AAV5-hSyn-HA-hM4Di in amygdala, one with AAV5-hSyn-HA-hM3Dq in amygdala, and  
620 one uninjected control. The data from the hM3Dq subject was not used in this study.

621

622 **[C<sup>11</sup>]DCZ Binding Image Analysis**

623 A parameter representing radioligand-receptor binding was calculated to serve as an index of  
624 neuroreceptor density. The distribution volume ratio (DVR) was estimated from the microPET  
625 time series for each voxel in this parametric image. The DVR images were calculated using the  
626 SRTM2 algorithm<sup>43, 44</sup> and the cerebellar grey matter as the reference region of negligible  
627 specific ligand-receptor binding. The DVR images were spatially transformed into a common T1-  
628 weighted MRI template space made from 592 rhesus monkeys<sup>7</sup> and blurred with a 2mm FWHM  
629 smoothing kernel using Advanced Normalization Tools (ANTs; <sup>84, 85</sup>). For the purpose of  
630 visualizing the presence of the hM4Di in the injected regions, the [<sup>11</sup>C]DCZ DVR images were  
631 then scaled such that the specific binding in the prefrontal cortex was matched across the  
632 images. This was done to normalize for overall global differences in DCZ-specific receptor  
633 expression across subjects, and the prefrontal cortex was selected because this region revealed  
634 the highest and most uniform values of [<sup>11</sup>C]DCZ DVR across subjects. The image from the  
635 control subject was then subtracted from each of the hM4Di DREADDs subjects and the  
636 average of these two difference images was then calculated using FSL (FMRIB). The unscaled  
637 microPET scanning data obtained with [<sup>11</sup>C]-DCZ will be uploaded to a public repository, for  
638 example <https://neurovault.org/>.

639

640 **Quantification and Statistical Analysis**

641 Autoradiographic data obtained from the [<sup>3</sup>H]clozapine binding assay were compared between  
642 the uninjected left hemisphere and the injected right hemisphere using a two-tailed unpaired t-  
643 test. In the initial dose response study to assess the effects of 0.1 mg/kg and 0.5 mg/kg  
644 clozapine on freezing, locomotion and experimenter orient during NEC, the durations were  
645 transformed ( $\log_{10} + 1$ ) and then analyzed by ANOVA, followed by Dunnett's multiple comparison  
646 test comparing results from the two clozapine doses to vehicle. To analyze the plasma ACTH  
647 and the cortisol data from the 8 animals that received vehicle and both the 0.03 mg/kg and 0.1

648 mg/kg doses of clozapine, repeated measures ANOVAs were used. *Post hoc* analysis was done  
649 with a Dunnett's multiple comparison test comparing the two doses of clozapine to vehicle. In  
650 these same 8 animals, to compare plasma clozapine and norclozapine levels that resulted from  
651 the 0.03 mg/kg and 0.1 mg/kg doses of clozapine, paired two tailed t-tests were performed. To  
652 analyze the behavioral data from the hM4Di-HA study, averaged freezing and locomotion  
653 duration were transformed ( $\log_{10} + 1$ ) and the averaged cooing frequency was square root  
654 transformed. Results from the vehicle condition were subtracted from the clozapine condition  
655 and the difference was analyzed using a two-way repeated measure ANOVA. In an additional  
656 analysis, the freezing data were residualized for plasma clozapine concentration and then  
657 analyzed with a two-way repeated measure ANOVA. *Post hoc* analysis was performed using  
658 Sidak's multiple comparison test. To compare plasma clozapine and norclozapine levels  
659 between the Control and hM4Di-HA DREADDs groups during postsurgical testing, the values  
660 obtained after the two HIP tests were averaged and compared using unpaired two tailed t-tests.  
661 All statistical testing was performed using either Prism v. 8.1 (GraphPad Software, San Diego,  
662 CA) or IBM SPSS Statistics v. 25 (IBM, Armonk, NY). Graphical representations of the data  
663 were prepared using Prism.

664

## 665 **Author contributions**

666 NHK, ASF, PHR, SALM, JAO, and MM conceptualized the study. NHK oversaw the  
667 study. JAO, VRE, MEO and MKR performed the surgeries. PHR performed the plasma  
668 endocrine assays, MAB determined plasma clozapine levels and JLG performed the *in vitro*  
669 autoradiography assays. MKR and VRE performed the behavioral data collection. PHR and JO  
670 analyzed the behavioral data and SALM performed the immunohistochemical microscopy and  
671 stereological analyses. AHD and BTC synthesized the PET ligand [<sup>11</sup>C]-DCZ and aided in

672 analysis of PET imaging data. PHR, SALM, JAO and NHK wrote the paper. All authors provided  
673 feedback.

674

## 675 **Acknowledgements**

676 We thank the personnel of the Harlow Center for Biological Psychology, the  
677 HealthEmotions Research Institute, the Waisman Laboratory for Brain Imaging and Behavior,  
678 the Wisconsin National Primate Research Center, the Wisconsin Institutes for Medical  
679 Research, K. Brunner, W. Block, E. Brodsky, A. Alexander, M. Emborg, E. Fekete, D. French,  
680 M. Rabska and H. VanValkenberg. Confocal microscopy was performed at University of  
681 Wisconsin-Madison (UW) Biochemistry Optical Core, which was established with support from  
682 the UW Department of Biochemistry Endowment. This work was supported by NIH grant R01-  
683 MH046729 to NHK, the Waisman Center (P30-HD003352) and the NIDA intramural research  
684 program (ZIA000069). Research reported in this publication was also supported in part by the  
685 Office Of The Director, National Institutes of Health under Award Number P51OD011106 to the  
686 Wisconsin National Primate Research Center, University of Wisconsin-Madison. In addition, this  
687 research was conducted in part at a facility constructed with support from Research Facilities  
688 Improvement Program grant numbers RR015459-01 and RR020141-01. The content is solely  
689 the responsibility of the authors and does not necessarily represent the official views of the  
690 National Institutes of Health. Preliminary versions of this work were presented in poster form at  
691 the Society for Neuroscience meeting in San Diego, CA, November 3-7, 2018, and the Society  
692 of Biological Psychiatry meeting in Chicago, IL, May 16-18, 2019.

693

694

695

696     **Declaration of Interests**

697           NHK currently receives research support from the National Institute of Mental Health;  
698       serves as a consultant to CME Outfitters, the Pritzker Neuro-psychiatric Disorders Research  
699       Consortium, Skyland Trail Advisory Board and the Institute of Early Adversity Research External  
700       Scientific Advisory Board at the University of Texas - Austin; is a share holder in Seattle  
701       Genetics; has served as co-editor of Psychoneuroendocrinology and currently serves as Editor-  
702       in-Chief of The American Journal of Psychiatry. All other authors report no biomedical financial  
703       interests or potential conflicts of interest.

## References

1. Kessler, RC, Aguilar-Gaxiola, S, Alonso, J, Chatterji, S, Lee, S, Ormel, J, et al. (2009). The global burden of mental disorders: an update from the WHO World Mental Health (WMH) surveys. *Epidemiol. Psichiatri. Soc.* 18, 23-33.
2. Kessler, RC, Ruscio, AM, Shear, K, and Wittchen, HU (2010). Epidemiology of anxiety disorders. *Curr. Top. Behav. Neurosci.* 2, 21-35.
3. Fox, AS, Shelton, SE, Oakes, TR, Davidson, RJ, and Kalin, NH (2008). Trait-like brain activity during adolescence predicts anxious temperament in primates. *PLoS One* 3, e2570.
4. Kalin, NH, Shelton, SE, Fox, AS, Oakes, TR, and Davidson, RJ (2005). Brain regions associated with the expression and contextual regulation of anxiety in primates. *Biol. Psychiatry* 58, 796-804.
5. Oler, JA, Fox, AS, Shelton, SE, Rogers, J, Dyer, TD, Davidson, RJ, et al. (2010). Amygdalar and hippocampal substrates of anxious temperament differ in their heritability. *Nature* 466, 864-868.
6. Alisch, RS, Chopra, P, Fox, AS, Chen, K, White, AT, Roseboom, PH, et al. (2014). Differentially methylated plasticity genes in the amygdala of young primates are linked to anxious temperament, an at risk phenotype for anxiety and depressive disorders. *J. Neurosci.* 34, 15548-15556.
7. Fox, AS, Oler, JA, Shackman, AJ, Shelton, SE, Raveendran, M, McKay, DR, et al. (2015). Intergenerational neural mediators of early-life anxious temperament. *Proc. Natl. Acad. Sci. U. S. A.* 112, 9118-9122.
8. Roseboom, PH, Nanda, SA, Fox, AS, Oler, JA, Shackman, AJ, Shelton, SE, et al. (2014). Neuropeptide Y receptor gene expression in the primate amygdala predicts anxious temperament and brain metabolism. *Biol. Psychiatry* 76, 850-857.
9. Shackman, AJ, Fox, AS, Oler, JA, Shelton, SE, Davidson, RJ, and Kalin, NH (2013). Neural mechanisms underlying heterogeneity in the presentation of anxious temperament. *Proc. Natl. Acad. Sci. U. S. A.* 110, 6145-6150.
10. Fox, AS, Oakes, TR, Shelton, SE, Converse, AK, Davidson, RJ, and Kalin, NH (2005). Calling for help is independently modulated by brain systems underlying goal-directed behavior and threat perception. *Proc. Natl. Acad. Sci. U. S. A.* 102, 4176-4179.
11. Fox, AS, Oler, JA, Shelton, SE, Nanda, SA, Davidson, RJ, Roseboom, PH, et al. (2012). Central amygdala nucleus (Ce) gene expression linked to increased trait-like Ce metabolism and anxious temperament in young primates. *Proc. Natl. Acad. Sci. U. S. A.* 109, 18108-18113.
12. Kalin, NH, and Shelton, SE (1989). Defensive behaviors in infant rhesus monkeys: environmental cues and neurochemical regulation. *Science* 243, 1718-1721.

13. Nelson, EE, and Winslow, JT (2009). Non-human primates: model animals for developmental psychopathology. *Neuropsychopharmacology* 34, 90-105.
14. Kalin, NH, and Shelton, SE (2003). Nonhuman primate models to study anxiety, emotion regulation, and psychopathology. *Ann. N. Y. Acad. Sci.* 1008, 189-200.
15. Birn, RM, Shackman, AJ, Oler, JA, Williams, LE, McFarlin, DR, Rogers, GM, et al. (2014). Evolutionarily conserved prefrontal-amyg达尔 dysfunction in early-life anxiety. *Mol. Psychiatry* 19, 915-922.
16. Tromp, DPM, Fox, AS, Oler, JA, Alexander, AL, and Kalin, NH (2019). The Relationship Between the Uncinate Fasciculus and Anxious Temperament Is Evolutionarily Conserved and Sexually Dimorphic. *Biol. Psychiatry* 86, 890-898.
17. Tromp, DPM, Williams, LE, Fox, AS, Oler, JA, Roseboom, PH, Rogers, GM, et al. (2019). Altered Uncinate Fasciculus Microstructure in Childhood Anxiety Disorders in Boys But Not Girls. *Am. J. Psychiatry* 176, 208-216.
18. Garbarini, N (2010). Primates as a model for research. *Dis. Model. Mech.* 3, 15-19.
19. Kalin, NH, Shelton, SE, and Davidson, RJ (2004). The role of the central nucleus of the amygdala in mediating fear and anxiety in the primate. *J. Neurosci.* 24, 5506-5515.
20. Armbruster, BN, Li, X, Pausch, MH, Herlitze, S, and Roth, BL (2007). Evolving the lock to fit the key to create a family of G protein-coupled receptors potently activated by an inert ligand. *Proc. Natl. Acad. Sci. U. S. A.* 104, 5163-5168.
21. Sternson, SM, and Roth, BL (2014). Chemogenetic tools to interrogate brain functions. *Annu. Rev. Neurosci.* 37, 387-407.
22. Roth, BL (2016). DREADDs for Neuroscientists. *Neuron* 89, 683-694.
23. Galvan, A, Raper, J, Hu, X, Pare, JF, Bonaventura, J, Richie, CT, et al. (2019). Ultrastructural localization of DREADDs in monkeys. *Eur. J. Neurosci.* 50, 2801-2813.
24. Fredericks, JM, Fujimoto, A, and Rudebeck, PH (2019). Trust, but verify: A cautionary tale of translating chemogenetic methods (A commentray on Galvan et al). *Eur. J. Neurosci.* 50, 2751-2754.
25. Eldridge, MA, Aguilar, BL, Baxter, MG, Bourne, JA, Cuzon Carlson, VC, Deverman, BE, et al. (2020). Workshop report: chemogenetic technology for systems neuroscience research in non-human primates 2016. OSF Preprints.
26. Eldridge, MA, Lerchner, W, Saunders, RC, Kaneko, H, Krausz, KW, Gonzalez, FJ, et al. (2016). Chemogenetic disconnection of monkey orbitofrontal and rhinal cortex reversibly disrupts reward value. *Nat. Neurosci.* 19, 37-39.
27. Grayson, DS, Bliss-Moreau, E, Machado, CJ, Bennett, J, Shen, K, Grant, KA, et al. (2016). The Rhesus Monkey Connectome Predicts Disrupted Functional Networks Resulting from Pharmacogenetic Inactivation of the Amygdala. *Neuron* 91, 453-466.

28. Nagai, Y, Kikuchi, E, Lerchner, W, Inoue, KI, Ji, B, Eldridge, MA, et al. (2016). PET imaging-guided chemogenetic silencing reveals a critical role of primate rostromedial caudate in reward evaluation. *Nat. Commun.* 7, 13605.
29. Upright, NA, Brookshire, SW, Schnebelen, W, Damatac, CG, Hof, PR, Browning, PGF, et al. (2018). Behavioral Effect of Chemogenetic Inhibition Is Directly Related to Receptor Transduction Levels in Rhesus Monkeys. *J. Neurosci.* 38, 7969-7975.
30. Bonaventura, J, Eldridge, MAG, Hu, F, Gomez, JL, Sanchez-Soto, M, Abramyan, AM, et al. (2019). High-potency ligands for DREADD imaging and activation in rodents and monkeys. *Nat. Commun.* 10, 4627.
31. Raper, J, Murphy, L, Richardson, R, Romm, Z, Kovacs-Balint, Z, Payne, C, et al. (2019). Chemogenetic Inhibition of the Amygdala Modulates Emotional Behavior Expression in Infant Rhesus Monkeys. *eNeuro* 6.
32. Upright, NA, and Baxter, MG (2020). Effect of chemogenetic actuator drugs on prefrontal cortex-dependent working memory in nonhuman primates. *Neuropsychopharmacology* 45, 1793-1798.
33. Hayashi, T, Akikawa, R, Kawasaki, K, Egawa, J, Minamimoto, T, Kobayashi, K, et al. (2020). Macaques Exhibit Implicit Gaze Bias Anticipating Others' False-Belief-Driven Actions via Medial Prefrontal Cortex. *Cell Rep.* 30, 4433-4444 e4435.
34. Nagai, Y, Miyakawa, N, Takuwa, H, Hori, Y, Oyama, K, Ji, B, et al. (2020). Deschloroclozapine, a potent and selective chemogenetic actuator enables rapid neuronal and behavioral modulations in mice and monkeys. *Nat. Neurosci.* 23, 1157-1167.
35. Wess, J, Nakajima, K, and Jain, S (2013). Novel designer receptors to probe GPCR signaling and physiology. *Trends Pharmacol. Sci.* 34, 385-392.
36. Gomez, JL, Bonaventura, J, Lesniak, W, Mathews, WB, Sysa-Shah, P, Rodriguez, LA, et al. (2017). Chemogenetics revealed: DREADD occupancy and activation via converted clozapine. *Science* 357, 503-507.
37. Raper, J, Morrison, RD, Daniels, JS, Howell, L, Bachevalier, J, Wichmann, T, et al. (2017). Metabolism and Distribution of Clozapine-N-oxide: Implications for Nonhuman Primate Chemogenetics. *ACS Chem. Neurosci.* 8, 1570-1576.
38. Chang, WH, Lin, SK, Lane, HY, Wei, FC, Hu, WH, Lam, YW, et al. (1998). Reversible metabolism of clozapine and clozapine N-oxide in schizophrenic patients. *Prog. Neuropsychopharmacol. Biol. Psychiatry* 22, 723-739.
39. Jann, MW, Lam, YW, and Chang, WH (1994). Rapid formation of clozapine in guinea-pigs and man following clozapine-N-oxide administration. *Arch. Int. Pharmacodyn. Ther.* 328, 243-250.
40. McLaren, DA, Browne, RW, Shaw, JK, Krishnan Radhakrishnan, S, Khare, P, Espana, RA, et al. (2016). Clozapine N-Oxide Administration Produces Behavioral Effects in Long-Evans Rats: Implications for Designing DREADD Experiments. *eNeuro* 3.

41. Manvich, DF, Webster, KA, Foster, SL, Farrell, MS, Ritchie, JC, Porter, JH, *et al.* (2018). The DREADD agonist clozapine N-oxide (CNO) is reverse-metabolized to clozapine and produces clozapine-like interoceptive stimulus effects in rats and mice. *Sci. Rep.* 8, 3840.
42. Ji, B, Kaneko, H, Minamimoto, T, Inoue, H, Takeuchi, H, Kumata, K, *et al.* (2016). Multimodal Imaging for DREADD-Expressing Neurons in Living Brain and Their Application to Implantation of iPSC-Derived Neural Progenitors. *J. Neurosci.* 36, 11544-11558.
43. Gunn, RN, Lammertsma, AA, Hume, SP, and Cunningham, VJ (1997). Parametric imaging of ligand-receptor binding in PET using a simplified reference region model. *Neuroimage* 6, 279-287.
44. Wu, Y, and Carson, RE (2002). Noise reduction in the simplified reference tissue model for neuroreceptor functional imaging. *J. Cereb. Blood Flow Metab.* 22, 1440-1452.
45. Wentur, CJ, and Lindsley, CW (2013). Classics in chemical neuroscience: clozapine. *ACS Chem. Neurosci.* 4, 1018-1025.
46. Yadav, PN, Abbas, AI, Farrell, MS, Setola, V, Sciaky, N, Huang, XP, *et al.* (2011). The presynaptic component of the serotonergic system is required for clozapine's efficacy. *Neuropsychopharmacology* 36, 638-651.
47. Machado, CJ, and Bachevalier, J (2008). Behavioral and hormonal reactivity to threat: effects of selective amygdala, hippocampal or orbital frontal lesions in monkeys. *Psychoneuroendocrinology* 33, 926-941.
48. Davis, M (2000). The role of the amygdala in conditioned and unconditioned fear and anxiety. In *The Amygdala: A Functional Analysis*, 2nd ed, 2nd edn., J. Aggleton, ed. (New York: Oxford), pp 213-287.
49. Agustin-Pavon, C, Braesicke, K, Shiba, Y, Santangelo, AM, Mikheenko, Y, Cockroft, G, *et al.* (2012). Lesions of ventrolateral prefrontal or anterior orbitofrontal cortex in primates heighten negative emotion. *Biol. Psychiatry* 72, 266-272.
50. Su, X, Kells, AP, Salegio, EA, Salegio, EA, Richardson, RM, Hadaczek, P, *et al.* (2010). Real-time MR imaging with Gadoteridol predicts distribution of transgenes after convection-enhanced delivery of AAV2 vectors. *Mol. Ther.* 18, 1490-1495.
51. Kalin, NH, Fox, AS, Kovner, R, Riedel, MK, Fekete, EM, Roseboom, PH, *et al.* (2016). Overexpressing corticotropin-releasing factor in the primate amygdala increases anxious temperament and alters its neural circuit. *Biol. Psychiatry* 80, 345-355.
52. Spampanato, J, Polepalli, J, and Sah, P (2011). Interneurons in the basolateral amygdala. *Neuropharmacology* 60, 765-773.
53. McDonald, AJ (1992). Cell types and intrinsic connections of the amygdala. In *The Amygdala: Neurobiological Aspects of Emotion, Memory, and Mental Dysfunction*, J.P. Aggleton, ed. (New York, NY: Wiley-Liss), pp 67-96.

54. McDonald, AJ, and Augustine, JR (1993). Localization of GABA-like immunoreactivity in the monkey amygdala. *Neuroscience* 52, 281-294.
55. Ghashghaei, HT, and Barbas, H (2002). Pathways for emotion: interactions of prefrontal and anterior temporal pathways in the amygdala of the rhesus monkey. *Neuroscience* 115, 1261-1279.
56. Timbie, C, Garcia-Cabezas, MA, Zikopoulos, B, and Barbas, H (2020). Organization of primate amygdalar-thalamic pathways for emotions. *PLoS Biol.* 18, e3000639.
57. Amaral, DG, and Price, JL (1984). Amygdalo-cortical projections in the monkey (*Macaca fascicularis*). *J. Comp. Neurol.* 230, 465-496.
58. Aggleton, JP, Wright, NF, Rosene, DL, and Saunders, RC (2015). Complementary patterns of direct amygdala and hippocampal projections to the macaque prefrontal cortex. *Cereb. Cortex* 25, 4351-4373.
59. Saunders, RC, Rosene, DL, and Van Hoesen, GW (1988). Comparison of the efferents of the amygdala and the hippocampal formation in the rhesus monkey: II. Reciprocal and non-reciprocal connections. *J. Comp. Neurol.* 271, 185-207.
60. Wang, J, and Barbas, H (2018). Specificity of Primate Amygdalar Pathways to Hippocampus. *J. Neurosci.* 38, 10019-10041.
61. Davis, M, and Whalen, PJ (2001). The amygdala: vigilance and emotion. *Mol. Psychiatry* 6, 13-34.
62. Duvarci, S, and Pare, D (2014). Amygdala microcircuits controlling learned fear. *Neuron* 82, 966-980.
63. Janak, PH, and Tye, KM (2015). From circuits to behaviour in the amygdala. *Nature* 517, 284-292.
64. McDonald, AJ (2020). Functional neuroanatomy of the basolateral amygdala: Neurons, neurotransmitters, and circuits. In *Handbook of Behavioral Neuroscience*, vol. 26, J.H. Urban and J.A. Rosenkranz, eds. (San Diego, CA: Elsevier), pp 1-38.
65. Ehrlich, I, Humeau, Y, Grenier, F, Ciocchi, S, Herry, C, and Luthi, A (2009). Amygdala inhibitory circuits and the control of fear memory. *Neuron* 62, 757-771.
66. Felix-Ortiz, AC, Beyeler, A, Seo, C, Leppla, CA, Wildes, CP, and Tye, KM (2013). BLA to vHPC inputs modulate anxiety-related behaviors. *Neuron* 79, 658-664.
67. Tye, KM, Prakash, R, Kim, SY, Fenno, LE, Grosenick, L, Zarabi, H, et al. (2011). Amygdala circuitry mediating reversible and bidirectional control of anxiety. *Nature* 471, 358-362.
68. Etkin, A, Prater, KE, Schatzberg, AF, Menon, V, and Greicius, MD (2009). Disrupted amygdalar subregion functional connectivity and evidence of a compensatory network in generalized anxiety disorder. *Arch. Gen. Psychiatry* 66, 1361-1372.

69. Fox, AS, Oler, JA, Tromp do, PM, Fudge, JL, and Kalin, NH (2015). Extending the amygdala in theories of threat processing. *Trends Neurosci.* 38, 319-329.
70. Oler, JA, Fox, AS, Shackman, AJ, and Kalin, NH (2016). The central nucleus of the amygdala is a critical substrate for individual differences in anxiety. In *Living Without an Amygdala*, D.G. Amaral and R. Adolphs, eds. (New York, NY: Guilford Press), pp 218-251.
71. Pare, D, Quirk, GJ, and Ledoux, JE (2004). New vistas on amygdala networks in conditioned fear. *J. Neurophysiol.* 92, 1-9.
72. Zikopoulos, B, John, YJ, Garcia-Cabezas, MA, Bunce, JG, and Barbas, H (2016). The intercalated nuclear complex of the primate amygdala. *Neuroscience* 330, 267-290.
73. Fox, AS, Souaiaia, T, Oler, JA, Kovner, R, Kim, JM, Nguyen, J, et al. (2019). Dorsal amygdala neurotrophin-3 decreases anxious temperament in primates. *Biol. Psychiatry* 86, 881-889.
74. Han, W, Tellez, LA, Rangel, MJ, Jr., Motta, SC, Zhang, X, Perez, IO, et al. (2017). Integrated Control of Predatory Hunting by the Central Nucleus of the Amygdala. *Cell* 168, 311-324 e318.
75. Hartley, ND, Gaulden, AD, Baldi, R, Winters, ND, Salimando, GJ, Rosas-Vidal, LE, et al. (2019). Dynamic remodeling of a basolateral-to-central amygdala glutamatergic circuit across fear states. *Nat. Neurosci.* 22, 2000-2012.
76. Steinberg, EE, Gore, F, Heifets, BD, Taylor, MD, Norville, ZC, Beier, KT, et al. (2020). Amygdala-Midbrain Connections Modulate Appetitive and Aversive Learning. *Neuron* 106, 1026-1043 e1029.
77. Kalin, NH (1993). The Neurobiology of Fear. *Sci. Am.* 268, 94-101.
78. Emborg, ME, Joers, V, Fisher, R, Brunner, K, Carter, V, Ross, C, et al. (2010). Intraoperative intracerebral MRI-guided navigation for accurate targeting in nonhuman primates. *Cell Transplant.* 19, 1587-1597.
79. Emborg, ME, Hurley, SA, Joers, V, Tromp do, PM, Swanson, CR, Ohshima-Hosoyama, S, et al. (2014). Titer and product affect the distribution of gene expression after intraputaminal convection-enhanced delivery. *Stereotact. Funct. Neurosurg.* 92, 182-194.
80. Amaral, DG, and Bassett, JL (1989). Cholinergic Innervation of the Monkey Amygdala: An Immunohistochemical Analysis with Antisera to Choline Acetyltransferase. *J. Comp. Neurol.* 281, 337-361.
81. Paxinos, G, Huang, X-F, Petrides, M, and Toga, AW (2009). The Rhesus Monkey Brain in Stereotaxic Coordinates, Academic Press, San Diego.
82. Jewett, DM (1992). A simple synthesis of [11C]methyl triflate. *Int. J. Rad. Appl. Instrum. A* 43, 1383-1385.

83. Larsen, P, Ulin, J, Dahlstrom, K, and Jensen, M (1997). Synthesis of [11C]iodomethane by iodination of [11C]methane. *Appl. Radiat. Isot.* 48, 153-157.
84. Avants, BB, Tustison, NJ, Song, G, Cook, PA, Klein, A, and Gee, JC (2011). A reproducible evaluation of ANTs similarity metric performance in brain image registration. *Neuroimage* 54, 2033-2044.
85. Avants, BB, Yushkevich, P, Pluta, J, Minkoff, D, Korczykowski, M, Detre, J, *et al.* (2010). The optimal template effect in hippocampus studies of diseased populations. *Neuroimage* 49, 2457-2466.

## Figure Legends

### Figure 1. Representative Images of hM4Di-HA Expression in the Rhesus Amygdala

**A)** The rhesus amygdala is composed of several nuclei, of which the Ce (medial and lateral divisions in purple) and basal nucleus (magnocellular and intermediate divisions in blue) were stereologically analyzed in subject P1. **B)** Co-labeling of NeuN (left panels; greyscale) and HA (middle panels; red) in subject P1 revealed that neuronal expression of hM4Di-HA varied between subregions of the amygdala, with little coexpression observed in the central nucleus (top panels) compared to the magnocellular and intermediate portions of the basal nucleus (bottom panels). Images are maximum intensity projections integrated across the Z-stack. Scalebar (white) is 50 µm. Panel A adapted with permission from Paxinos et al., 2009.<sup>81</sup>

### Figure 2. Autoradiographic Demonstration of hM4Di-HA Expression in the Rhesus Amygdala

**A)** Autoradiograms from subject P2 unilaterally injected with AAV5-hSyn-HA-hM4Di (hM4Di-HA) into the amygdala, showing nonspecific and total [<sup>3</sup>H]clozapine (3.5 nM) binding. The white dotted line depicts the amygdala boundaries. **B)** Densitometric quantification of specific binding ([<sup>3</sup>H] clozapine total binding – nonspecific: total binding was assessed in three coronal slices) in the viral-infected amygdala compared to the uninfected amygdala.

### Figure 3. Effects of Clozapine Administration on Freezing Behavior During NEC

Log transformed freezing duration following administration of vehicle or two different doses of clozapine (n=5/group). Compared to Vehicle, there was a significant reduction in freezing duration following 0.5 mg/kg clozapine but not 0.1 mg/kg clozapine (\*\*p < 0.01).

**Figure 4. Effects of 0.03 mg/kg and 0.1 mg/kg Clozapine on Plasma ACTH and Cortisol Levels in Animals Selected for the DREADD Behavioral Experiment**

As part of characterizing individual doses of clozapine, effects on ACTH (upper) and cortisol (lower) were assessed following administration of vehicle, 0.03, and 0.1 mg/kg clozapine to the same animals (n=8). ACTH was significantly reduced by both doses, whereas significant reductions in cortisol occurred at the higher dose (\*p < 0.05, \*\*p < 0.01).

**Figure 5. DREADDs Experiment Methods**

**A)** Timeline for behavioral testing of monkeys receiving AAV5-hSyn-HA-hM4Di (n=5) and cage-mate controls (n=5). **B)** Overlap of the infused area across all subjects as assessed by the gadolinium signal detected with MRI. The colors represent the number of animals with gadolinium signal at each voxel. The overlap of the gadolinium injection clouds across all five experimental animals is depicted in yellow demonstrating consistent coverage of the dorsal amygdala region using the MRI-guided targeted injection procedure. **C)** Neurons expressing hM4Di-HA in a section containing the accessory basal nucleus in a maximum intensity projection image at 40X integrated across the Z-stack. Neurons are identified with NeuN in grey, and hM4Di-HA expression with HA immunoreactivity in red. Note, the neuron seen in center of the field of view is prominently expressing hM4Di-HA in its soma as well as in its neuronal extensions.

**Figure 6. [<sup>11</sup>C]DCZ Binding in the Amygdala Demonstrates hM4Di-HA Expression *In vivo***

The average difference (hM4Di-HA minus control) in [<sup>11</sup>C]DCZ binding signal from two of the hM4Di-HA animals in the DREADDs behavioral experiment is overlayed on a rhesus monkey brain MRI template. The average difference image is thresholded at 40%. Greater binding is observed bilaterally in the amygdala, where the AAV5-hSyn-HA-hM4Di construct was infused and where gadolinium signal was observed across all five hM4Di-HA subjects. The peak

difference in the right amygdala reached 53% greater binding signal in the hM4Di-HA animals. No other brain regions exceeded this threshold. See also Supplemental Figure 2.

**Figure 7. Quantification of hM4Di-HA Expression in the Amygdala**

**A)** Intraoperative MRI image of the gadolinium signal after the infusion into the dorsal amygdala of AAV5-hSyn-HA-hM4Di mixed with gadolinium. **B)** Acetylcholinesterase staining of a tissue section containing the amygdala from subject E1, demonstrating considerable staining in the basal nucleus and a lack of staining in the central nucleus. **C)** A depiction of the amygdala nuclei as derived from acetylcholinesterase staining. The box outlined in red represents the region of one of the sections that was used in the stereological analysis. **D)** A 200 x 200 x 10  $\mu\text{m}$  subregion within the accessory basal nucleus that was part of the stereological analysis, which is a magnification of the green square in panel E. Red fluorescence indicates HA immunoreactivity, and grey fluorescence indicates NeuN immunoreactivity. **E)** A tissue section used for stereological assessment of the co-expression of HA (red) and NeuN (greyscale). White squares indicate subregions where co-expression was quantified. **F)** A heat map of the percent of neurons, identified with NeuN, that are co-expressing HA, reflecting the stereological analysis performed on the section depicted in panel E. See also Supplemental Figure 3.

**Figure 8. DREADD-induced Change in Anxiety-related Behavioral Response**

The clozapine-induced change in freezing duration (Clozapine-Vehicle) occurring during the NEC component of the HIP for the hM4Di-HA and Control animals. The five different symbols each identify an hM4Di-HA subject and its cage-mate control. Symbols in black represent the difference between clozapine and vehicle at baseline prior to surgery (Pre). Symbols in red represent the difference between clozapine and vehicle after hM4Di-HA expression that is averaged across the two rounds of testing (Post). A significant Group by Session (Pre/Post) interaction was observed ( $F_{1,8} = 14.89$ ,  $p < 0.01$ ). Post hoc testing revealed a significantly

greater decrease in freezing for the hM4Di-HA animals Post compared to Pre (\*\*, p < 0.01); whereas the Control animals did not significantly differ Post compared to Pre.

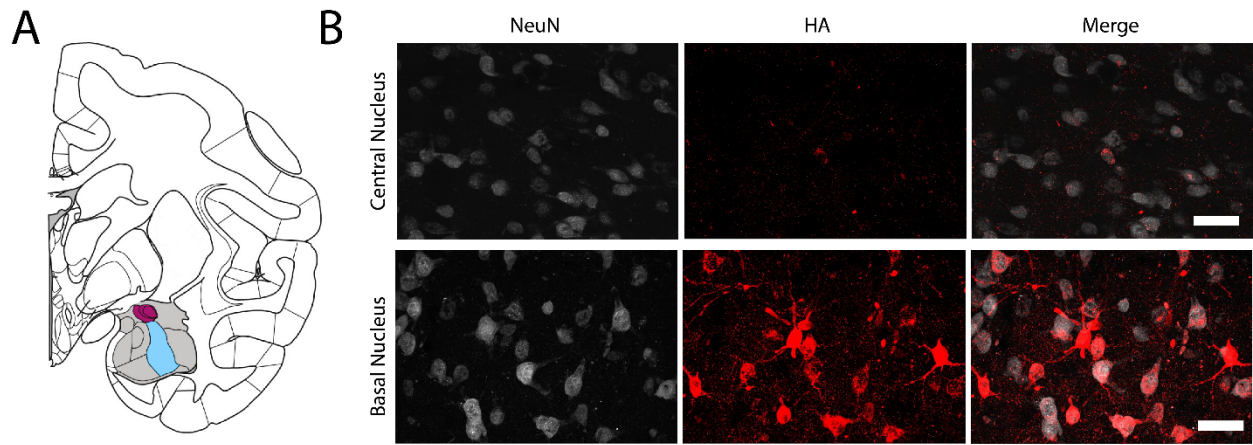


Figure 1

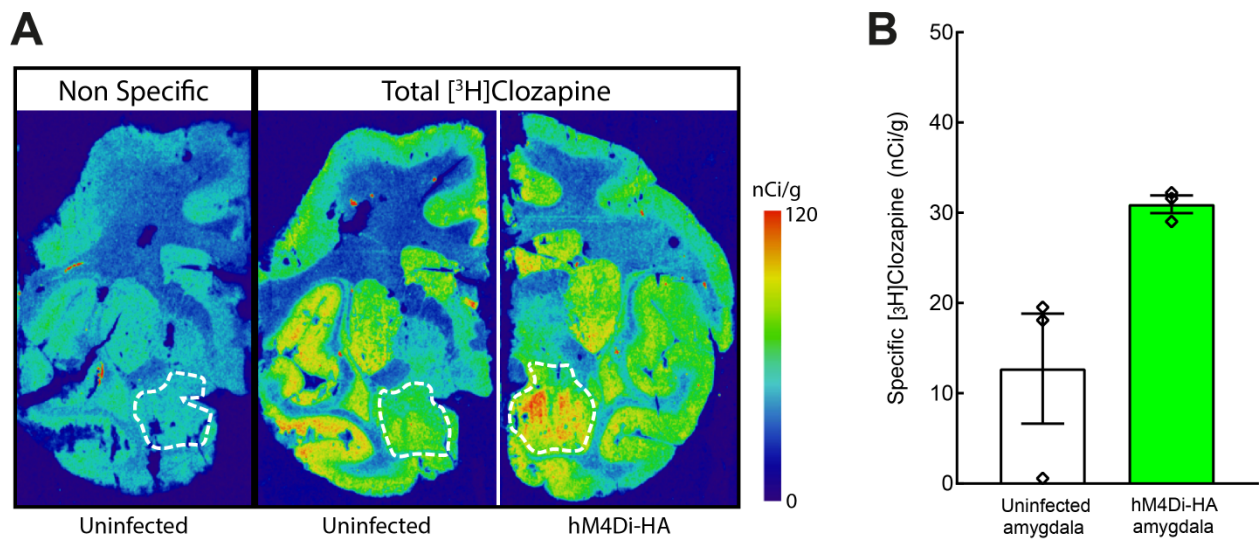


Figure 2

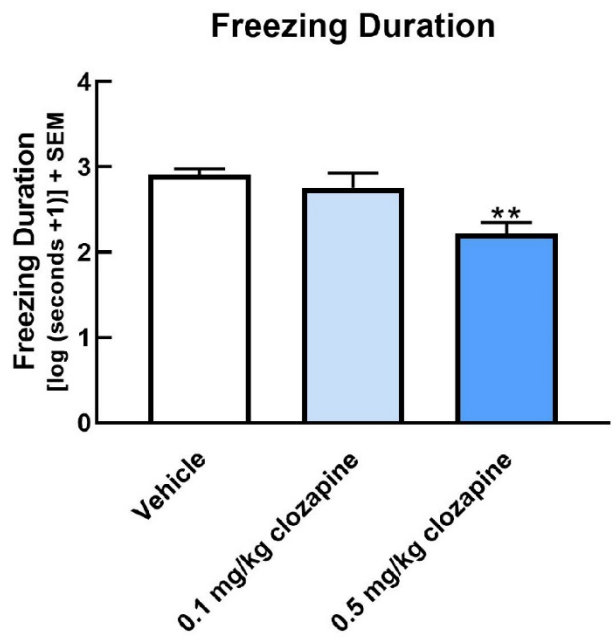


Figure 3

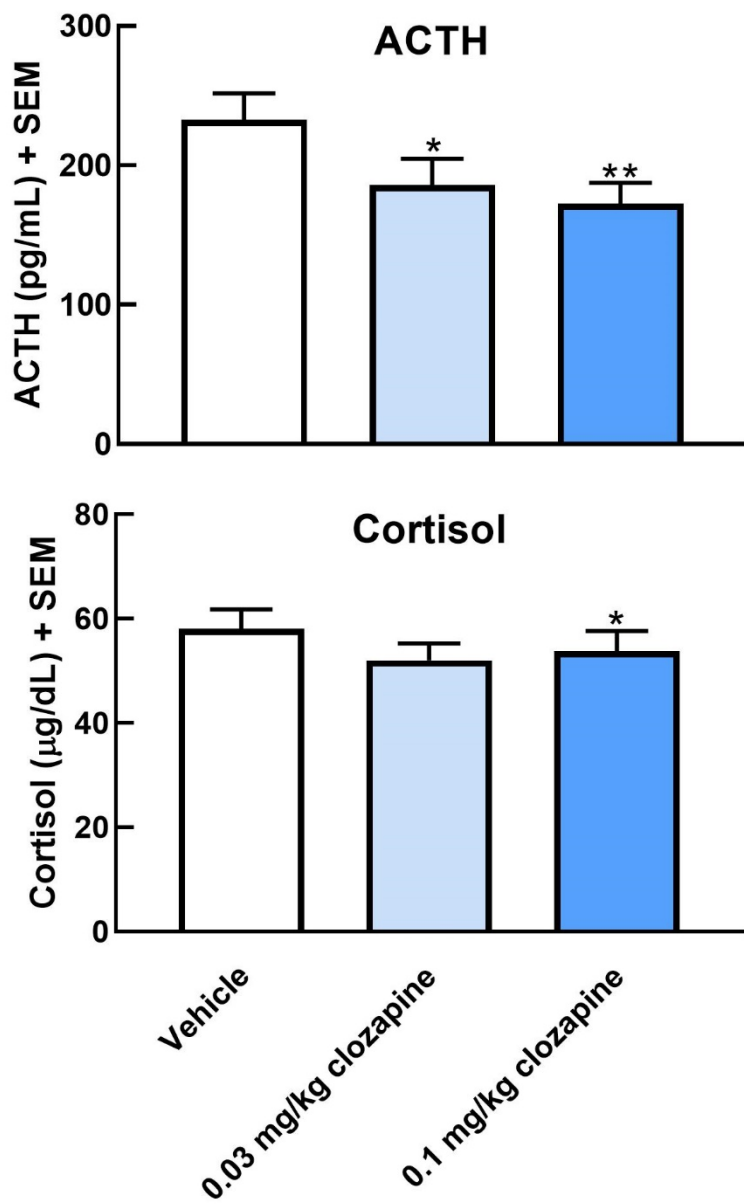


Figure 4

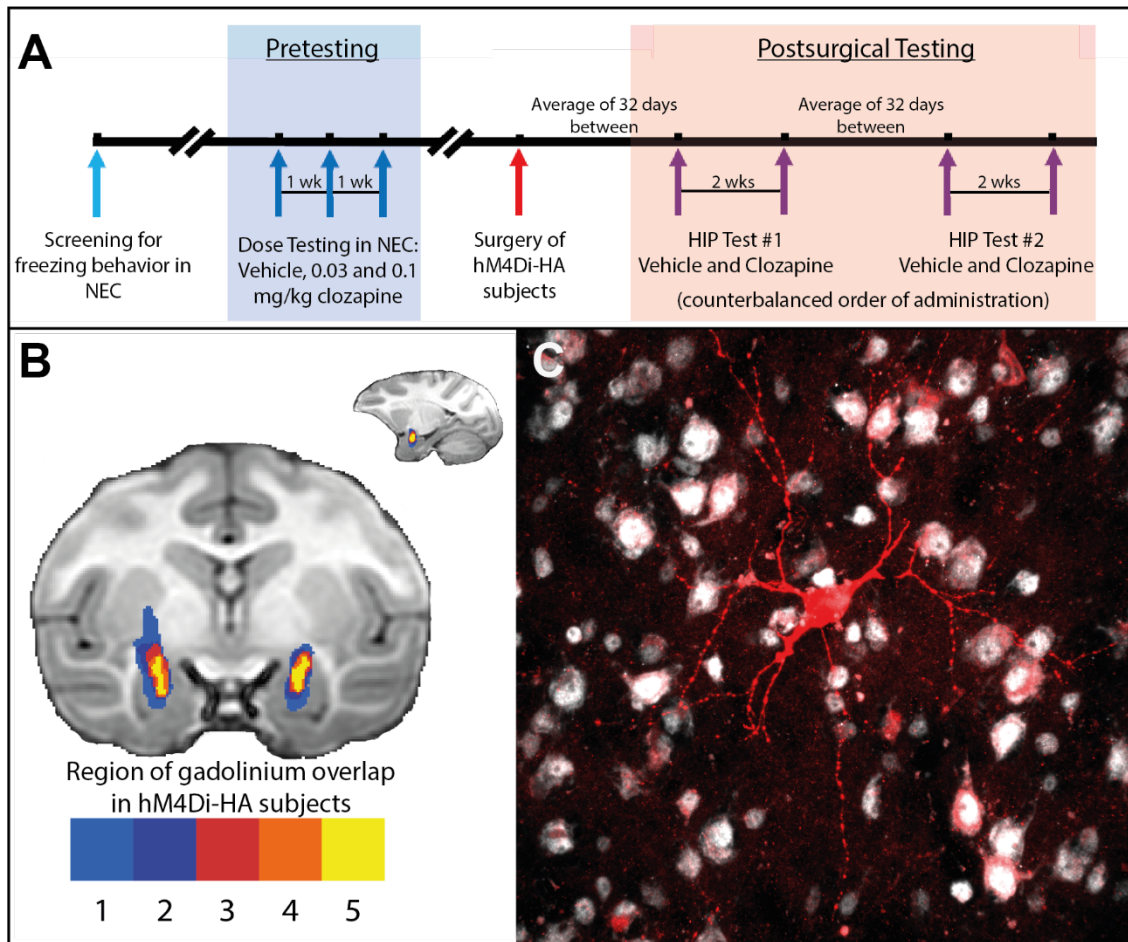


Figure 5

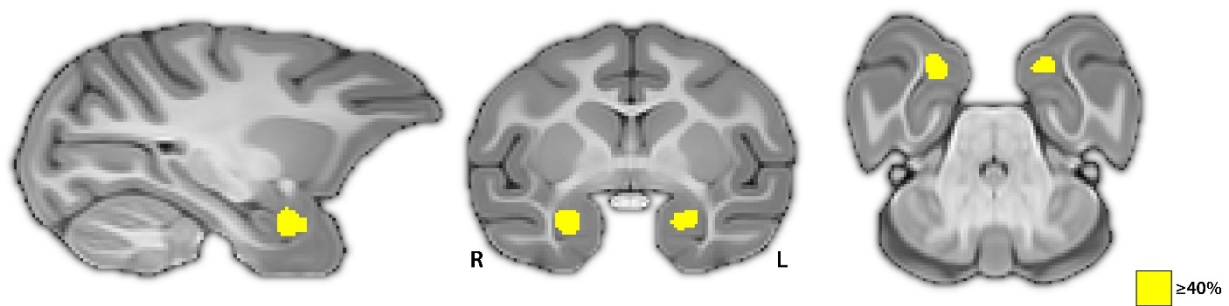


Figure 6

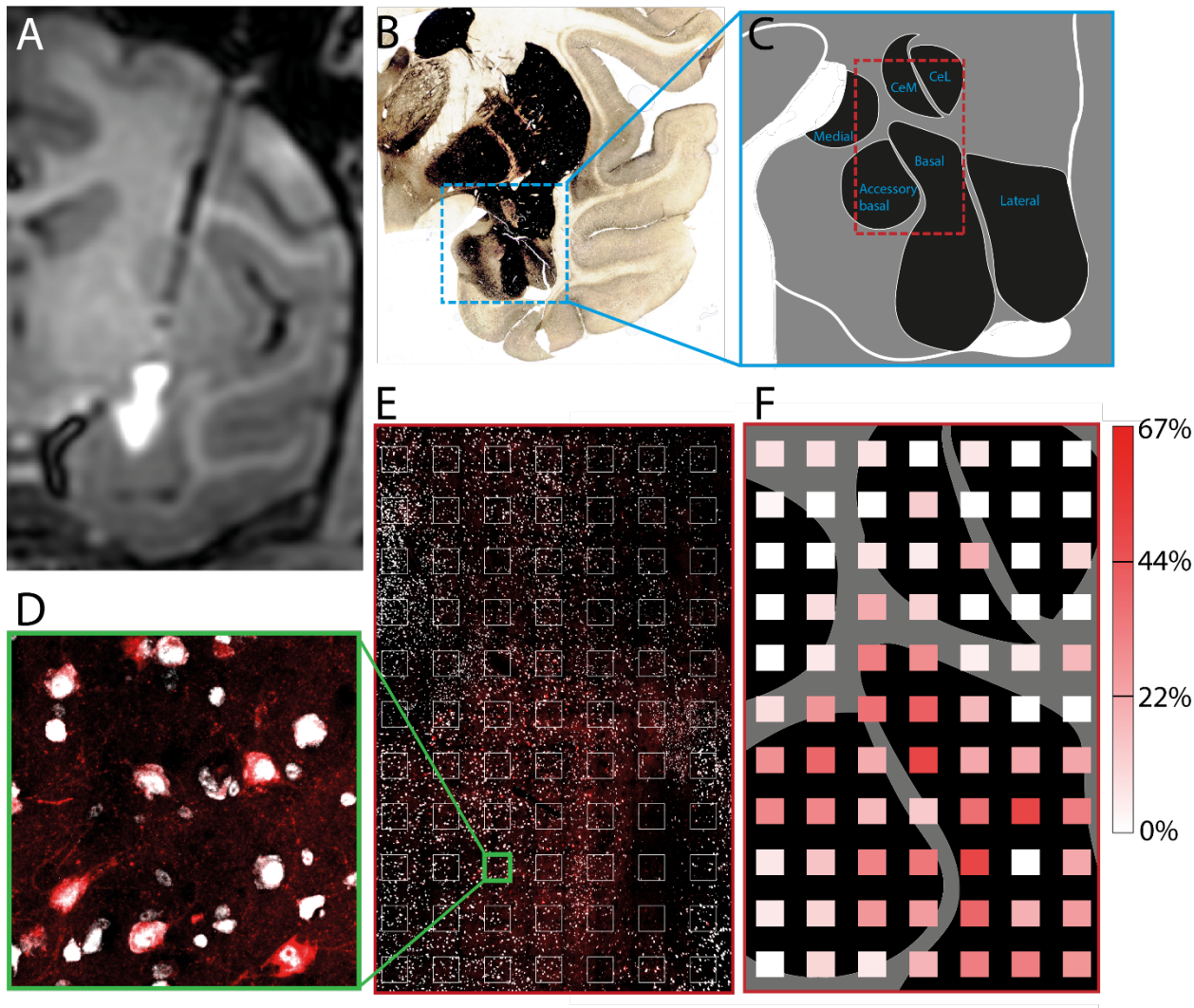


Figure 7

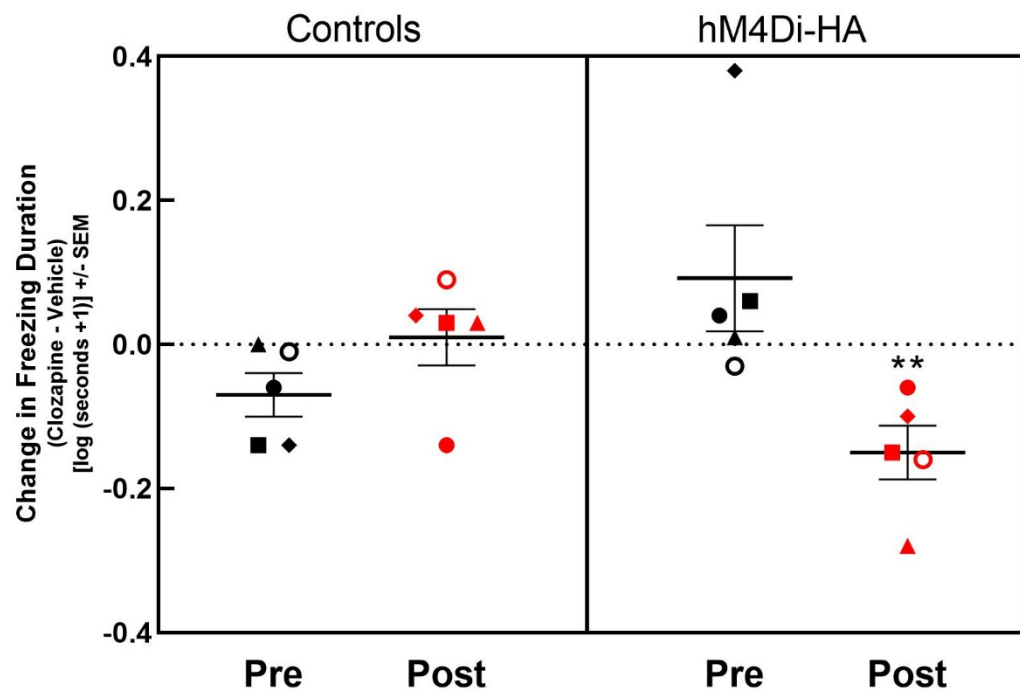


Figure 8